nature climate change

Article

https://doi.org/10.1038/s41558-023-01874-3

Responses of soil organic carbon to climate extremes under warming across global biomes

Received: 4 April 2023

Accepted: 19 October 2023

Published online: 22 December 2023

Check for updates

Mingming Wang[1,2], Shuai Zhang[1,2], Xiaowei Guo[1,2], Liujun Xiao[3], Yuanhe Yang[4], Yiqi Luo[5], Umakant Mishra[6] & Zhongkui Luo[1,2]

The impact of more extreme climate conditions under global warming on soil organic carbon (SOC) dynamics remains unquantified. Here we estimate the response of SOC to climate extreme shifts under 1.5 °C warming by combining a space-for-time substitution approach and global SOC measurements (0–30 cm soil). Most extremes (22 out of 33 assessed extreme types) exacerbate SOC loss under warming globally, but their effects vary among ecosystems. Only decreasing duration of cold spells exerts consistent positive effects, and increasing extreme wet days exerts negative effects in all ecosystems. Temperate grasslands and croplands negatively respond to most extremes, while positive responses are dominant in temperate and boreal forests and deserts. In tundra, 21 extremes show neutral effects, but 11 extremes show negative effects with stronger magnitude than in other ecosystems. Our results reveal distinct, biome-specific effects of climate extremes on SOC dynamics, promoting more reliable SOC projection under climate change.

Both mean climate (for example, average warming) and the frequency and intensity of climate extremes (for example, more heatwaves and droughts) are shifting across the globe[1]. This shift would substantially impact terrestrial carbon balance due to strong carbon cycle-climate feedbacks[2,3]. Satellite-based observations and global observation networks (for example, FLUXNET) have shown evidence that even a single climate extreme event can cause large reduction in regional ecosystem production and its effects are usually time lagged or last for years up to decades[4–6]. However, the relatively short-term nature of satellite-based and site-level records (for example, satellite observation was only available from the 1980s) is incapable of predicting the long-term consequences of climate extreme shifts on the global carbon cycle[2,7].

Among terrestrial carbon pools of the global carbon cycle, soil organic carbon (SOC) is the largest pool and contains more than twice the carbon stored in vegetation biomass and the atmosphere[8]. Although the response of SOC to mean climate changes such as warming has been extensively studied using modelling and experimental approaches[9], the role of accompanied shifts of climate extremes in regulating such a response has rarely been quantified based on observational data, particularly across large spatio-temporal extents[2]. A major challenge is that SOC changes would only be detectable or fully manifested at the timescale of SOC turnover, which is usually decadal or even centurial in most soils[10]. For this reason, observations after one or several extreme events occurring in a typical year or short period cannot fully capture long-term impacts of more extreme climate on SOC dynamics. Furthermore, replicating climate extremes in experiments is challenging, and different extremes (for example, droughts and heatwaves) may

[1]Key Laboratory of Agricultural Remote Sensing and Information Technology (Zhejiang Province), College of Environmental and Resource Sciences, Zhejiang University, Hangzhou, China. [2]Key Laboratory of Environment Remediation and Ecological Health, Ministry of Education, Zhejiang University, Hangzhou, China. [3]College of Agriculture, Nanjing Agricultural University, Nanjing, China. [4]State Key Laboratory of Vegetation and Environmental Change, Institute of Botany, Chinese Academy of Sciences, Beijing, China. [5]School of Integrative Plant Science, Cornell University, Ithaca, NY, USA. [6]Computational Biology and Biophysics, Sandia National Laboratories, Livermore, CA, USA. e-mail: luozk@zju.edu.cn

elicit distinct responses in soil carbon fluxes, potentially altering SOC balance[11,12].

Climate extremes exert influence on SOC dynamics at various temporal scales. In the short term, events such as heavy precipitation can lead to soil waterlogging, inhibiting microbial decomposition and/or causing spatial redistribution of SOC through erosion[13,14]. Drought alters carbon inputs to the soil in terms of their amount, quality and timing through its effect on plant growth and soil hydrothermal regimes[7,15]. Heatwaves can accelerate SOC decomposition[16], but are often accompanied by drought, resulting in a complex effect on SOC. Over the long term, different climate extremes can bring about a series of ecological and environmental shifts[2] such as: (1) changes in soil physiochemical environment (for example, soil aggregate transformation and stabilization, hydrophobicity), (2) alterations in plant, soil microbial and animal community composition and functionality[2,17] and (3) impacts on soil hydrology and nutrient cycling[18]. Overall, shifts in climate extremes may directly or indirectly influence long-term SOC dynamics depending on local environmental conditions and the specific type of climate extreme[12].

Here we quantify the response of SOC to shifts of various climate extremes that are projected under future climate[19,20]. This quantification builds upon SOC stock (kg m^{-2}) measurements in 0–30 cm of topsoil at 113,013 sites across the globe (ref. 21; Supplementary Fig. 1), along with eight indices representing the magnitude and frequency of different extreme events (Supplementary Fig. 2 and Supplementary Table 1). These events include heatwaves, cold waves, extreme dry and wet days from a global map product derived by the Expert Team on Climate Change Detection and Indices[22,23]. Another 25 indices were also obtained from the same map product, reflecting the threshold and probability of temperature- and precipitation-related extremes based on long-term climate records[24] (Supplementary Table 1). Using the data, a hybrid approach combining space-for-time substitution and meta-analysis techniques[21] (Fig. 1) was used to estimate the responses of SOC to two general climate change scenarios: a warmer climate without extreme shifts (W, that is, only mean annual temperature is increased, which is assigned to 1.5 °C in this study) and a warmer and more extreme climate (W + E, 1.5 °C warming plus more extreme climate; Fig. 1). Uncertainties in future climate extremes[25] were considered by using a five-level change gradient for each of the 33 climate extreme indices (CEIs) (Supplementary Table 1). Compound extreme events (that is, concurrent occurrence of multiple climate extremes) may also be more common in the future[26] but are more difficult to predict. To demonstrate their importance, here we illustrate the influence of shifts in two compound extremes involving two widely recognized individual extremes: heatwave + extreme dry and heatwave + extreme wet (Methods).

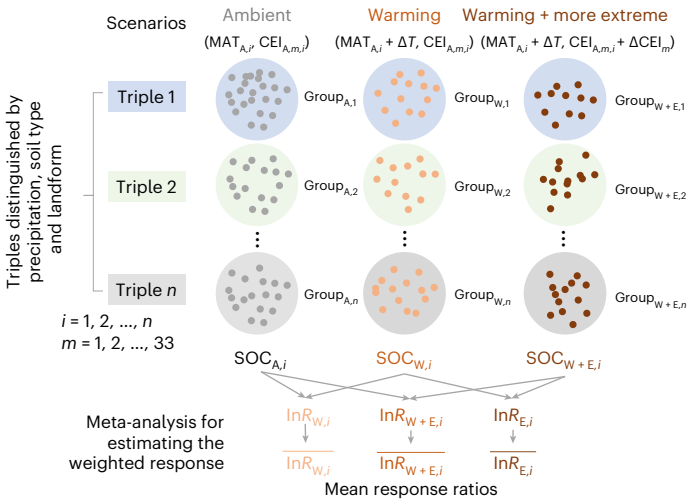

Fig. 1 | Schematic representation of the approach used to quantify the response of SOC to climate extreme and warming scenarios. Each dot represents one SOC observation. Dots in the *i*th plate share the same mean annual temperature ($MAT_{A,i}$) and the frequency or intensity of the *m*th climate extreme ($CEI_{A,m,i}$), while dots in the same colour plates indicate a triple sharing the same mean annual precipitation (MAP), precipitation seasonality, landform and soil type. ΔCEI_m (shown in Supplementary Table 1) and ΔT (1.5 °C in this study) are changes in $CEI_{A,m}$ and MAT_A of interest, respectively. SOC values in the warming (W) and warming plus more extreme (W + E) plates are compared with the values in the ambient (A) plates in the same triple to calculate a weighted average effect size (that is, the response of SOC to ΔT and $\Delta T + \Delta CEI_m$) by the inverse of the sum of within- and between-group variances, using meta-analytic techniques. The response of SOC to W + E attributed to climate extremes is calculated by the comparison between W and W + E plates with meta-analysis (Methods). Figure adapted with permission from ref. 21, Springer Nature Limited.

Climate extremes diversify the response of SOC to warming

Averaging across the globe, SOC is reduced by 10.5% (8.1–12.3%, 95% confidence interval) under 1.5 °C warming (that is, W, Fig. 2 and Extended Data Fig. 1), consistent with our previous estimate at a similar warming level[21]. However, this SOC reduction is significantly altered by shifts in climate extremes (Fig. 2 and Extended Data Fig. 1). For 8 out of 33 CEIs (heatwave frequency, extreme wet magnitude, extreme wet frequency, extreme dry magnitude, max daily minimum temperature, maximum daily precipitation, maximum precipitation of 5 consecutive days, precipitation intensity), more extreme conditions consistently exacerbate SOC reduction (that is, additional SOC reduction; Fig. 2 and Extended Data Fig. 1), with the additional reduction increasing with higher extreme levels (Fig. 2 and Extended Data Fig. 1). For example, SOC reduction increases from 2% with a 2-day increase in heatwave frequency to 21% with a 10-day increase (Fig. 2). On the contrary, SOC reduction is consistently attenuated or even reversed for two extremes (cold wave magnitude and coldest daily minimum temperature), offsetting the negative effect of warming on SOC under more extreme conditions (Fig. 2 and Extended Data Fig. 1).

Several CEIs exhibit a threshold or turning point regarding the rate or direction of warming-induced SOC changes (Fig. 2 and Extended Data Fig. 1). Specifically, a decrease in cold wave frequency (CWF) initially leads to less SOC reduction until reaching a turning point of a 4-day decrease after which further decrease in CWF results in more SOC reduction (Fig. 2). A similar pattern is also detected for the length of summer days, the number of cool days and nights and the number of hot (tropical) nights (Extended Data Fig. 1). For some other CEIs (that is, extreme dry frequency, min daily maximum temperature, max daily minimum temperature, growing season length, number of icing days, heavy precipitation, consecutive wet days), SOC changes have an apparent peak at certain CEI changes (Fig. 2 and Extended Data Fig. 1). These varied SOC responses may stem from trade-offs between changes in carbon inputs to soil and decomposition of SOC under more extreme climate[27–29] or distinct effects of climate extreme shifts on different ecosystem processes (for example, microbial carbon use efficiency[30]) related to SOC dynamics. For instance, the decrease of cold wave frequency may not only benefit plant growth thereby enhancing carbon inputs to soil but also stimulate microbial decomposition. The net effects on SOC balance depend on the proportionate changes in carbon inputs and outputs.

The responses of SOC to single extremes such as heatwave, extreme dry and extreme wet are not significantly different from the responses to their compound events at their low-level changes (that is, 20% increase in their frequency; Fig. 2b). However, at high-level changes (that is, 40% increase in frequency) of both individual events, compound heatwave and extreme dry (HWF + EDF) leads to an additional

https://doi.org/10.1038/s41558-023-01874-3

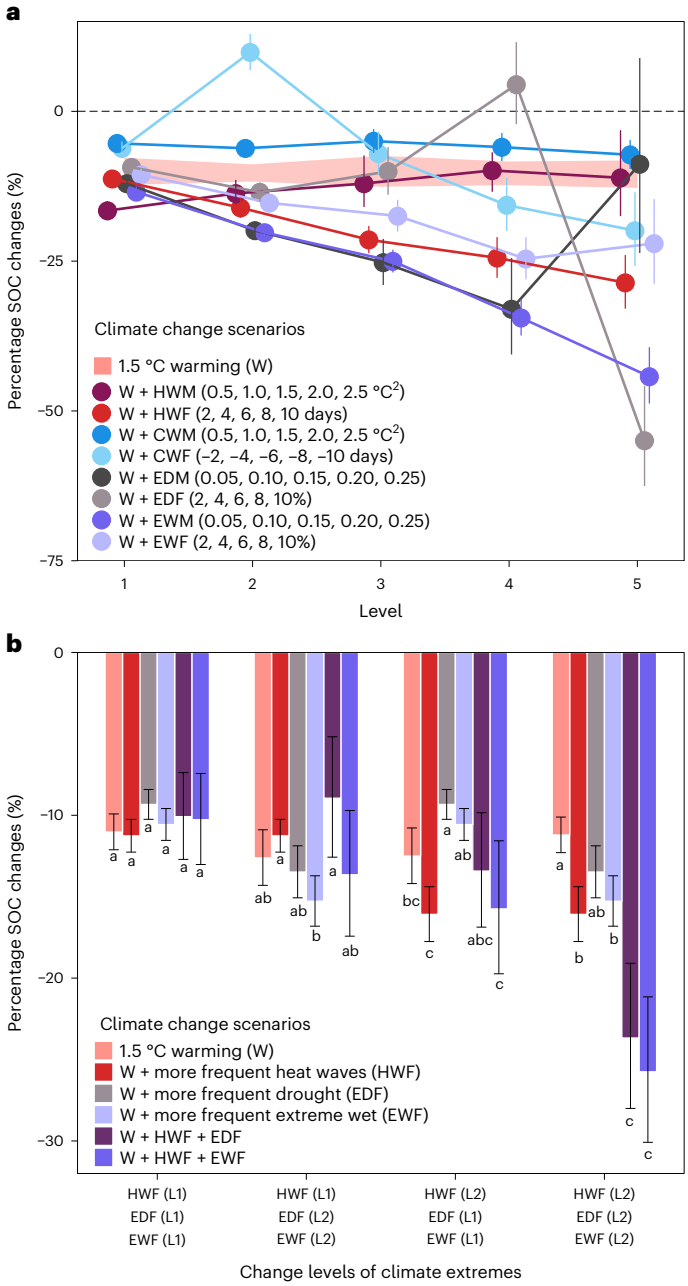

Fig. 2 | Global responses of SOC to climate change scenarios. a, Responses to eight integrated climate extremes. HWM and HWF, the magnitude and frequency of heatwaves, respectively; CWM and CWF, the magnitude and frequency of cold waves, respectively; EWM and EWF, the magnitude and frequency of extreme wet, respectively; EDM and EDF, the magnitude and frequency of extreme dry, respectively. Numbers in the parentheses show the five change levels. **b**, Responses to compound climate extremes. Two levels of climate extreme changes with their selected combinations (due to data limitation) are assessed. Different letters in the same group of comparisons indicate significant difference between climate change scenarios. A symbol of '+' indicates concurrent occurrence of the relevant changes. Error bars show 95% confidence interval, centred on the mean. Supplementary Table 1 provides the detailed definition of climate extremes, and Supplementary Tables 4 and 5 provide sample size and other statistics of **a** and **b**, respectively.

13% SOC reduction, whereas heatwave and extreme dry events individually only lead to additional 2% and 5% SOC reduction, respectively (Fig. 2b). Similarly, additional SOC reduction induced by compound heatwave and extreme wet events is nearly double compared with that induced by single shifts of heatwave or extreme wet under high-level changes (Fig. 2b). These results demonstrate that compound climate extremes may cause more SOC reduction under warming (especially at high-level changes) and have a more profound and complex impacts compared to single extremes.

Global average SOC changes induced by climate extremes

We estimated percentage SOC changes attributed to climate extremes (ΔSOC_E) under the W + E scenario by calculating the difference between the percentage responses to W + E and to W. Then, a linear mixed-effects model with biome-dependent slopes but without intercept (that is, additional change should be zero under zero climate extreme changes) was fitted to infer the relationship of ΔSOC_E with climate extreme change levels. The regression slopes can be also explained as the percentage of additional SOC changes induced by unit changes in climate extremes.

On average, ΔSOC_E shows distinct relationships with the 33 CEIs in terms of both magnitude and direction (that is, the regression slopes for the fixed effect of climate extremes; Fig. 3a). Negative relationships are dominant (22 out of 33). However, only the length of hot (tropical) nights (TR), cold-spell duration index, extreme dry magnitude (EDM) and extreme wet magnitude (EWM) exert significant linear effects (that is, the regression slope is significantly different from zero) on ΔSOC_E (Fig. 3a). Specifically, the slope for TR is −8%, that is, additional percentage of SOC reduction is 8% for every 5-day increase of TR. SOC increases by 22% per 5-day decrease of cold-spell duration index. For EWM, SOC decreases by 7% per 0.1 unit increase of EWM and some other CEIs related to extreme precipitation magnitude also show negative effects on SOC. Positive relationships between SOC and climate extremes mainly occur for extremes related to shortening of low temperature days such as frost days and cold spells (Fig. 3a). In addition, the increase of low temperature-related extremes represented by daytime and nighttime minimum temperature has positive effects, whereas CEIs related to high temperature extremes show negative effects, especially the maximum and range of daily temperature. For EDM, every 0.1 unit increase leads to additional 16% SOC reduction, and the extreme dry frequency also shows a negative effect (Fig. 3a).

Biome-specific SOC changes induced by climate extremes

SOC in different ecosystems show distinct responses to climate extremes (Fig. 3b and Extended Data Fig. 2). In temperate grasslands and croplands, SOC is negatively influenced by most climate extremes assessed (23 and 20 out of 33, respectively), followed by tropical/subtropical forests (16 out of 33; Fig. 3b). The impacts of climate extremes on SOC in croplands may be modulated by management intervention. Irrigation, for example, may stimulate SOC decomposition via its positive effects on soil moisture. Besides, many crop varieties are genetically selected for high production in optimal conditions, so they would be more sensitive to extreme events[31]. In other ecosystems except tundra, positive effects are more common (Fig. 3b). Especially, only four CEIs show significant negative effects in boreal forests. In tundra, 21 CEIs exert neutral (that is, insignificant) effects, while only decreasing cold wave magnitude shows positive influence. The remaining 11 extremes show negative effects, and, more importantly, the magnitude of most effects is much stronger in tundra than their corresponding effects in other ecosystems (Fig. 3b and Extended Data Fig. 2). Tundra has been suggested to be the most vulnerable ecosystem to climate change[32,33]. More extreme climate may worsen the vulnerability of SOC stocks in tundra.

The same climate extreme exerts distinct effects on SOC across ecosystems (Fig. 3b and Extended Data Fig. 2). For example, increase of heatwave magnitude has significant negative effect on ΔSOC_E in tropical/subtropical ecosystems (forests and grasslands/savannahs) but positive in temperate forest, Mediterranean/montane shrublands and croplands (Extended Data Fig. 2). Increase of extreme dry frequency

https://doi.org/10.1038/s41558-023-01874-3

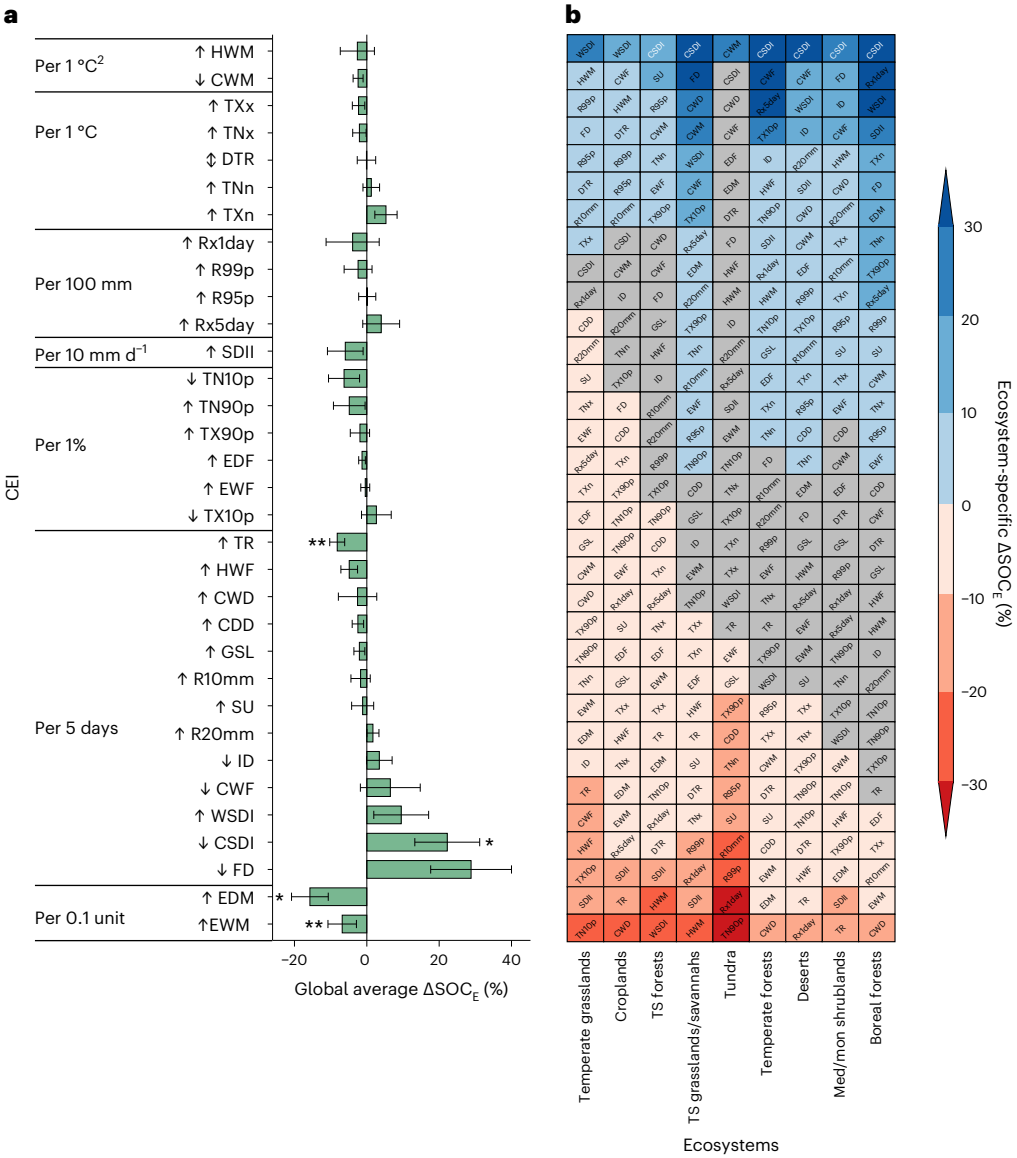

Fig. 3 | The dependence of additional ΔSOC_E on change levels of climate extremes under warming. ΔSOC_E is defined as the difference between percentage responses of SOC to W + E (1.5 °C warming plus more extreme climate) and that to W (1.5 °C warming), which can also be explained as SOC changes attributed to climate extremes under W + E. ↑, ↓ and ↕ beside each CEI represent that the CEI is increased, decreased or either under warming, respectively. **a**, Global average dependence. Error bars show one standard error, centred on the mean. Supplementary Table 6 shows the relevant sample size and other statistics. **, $P < 0.01$; *, $P < 0.05$. **b**, Ecosystem-specific dependence. Grey grids indicate that the estimated dependence is statistically insignificant ($P > 0.05$). TS forests, tropical/subtropical forests; Med/mon shrublands, Mediterranean/montane shrublands; TS grasslands/savannas, tropical/subtropical grasslands/savannas. Detailed descriptions of CEIs are shown in Supplementary Table 1.

negatively influences ΔSOC_E in five ecosystems but positively in temperate forest and deserts. In addition, for the same type of extreme, the changes of its frequency and magnitude (that is, the intensity or severity of one event) have different consequences on ΔSOC_E (Extended Data Fig. 2). For example, unlike the positive effects of extreme dry frequency in temperate forests and deserts, the positive effect of extreme dry magnitude occurs in boreal forests and tropical/subtropical grasslands/savannahs. It is noteworthy that cold-spell duration and extreme wet magnitude are the only two CEIs showing consistent positive and negative effects (if the effect is significant) on SOC in all ecosystems, respectively (Extended Data Fig. 2).

Comparison with field experiments

Drought is the most experimentally explored climate extreme in terms of its effect on ecosystem carbon balance, albeit experimental duration is relatively short[18]. We compared our estimates to a recent meta-analysis synthesizing global drought experiments[18] (Extended Data Fig. 3). We integrated ΔSOC_E induced by EDM into relevant three general ecosystems to conduct a comparison with field drought experiments (limited observational data do not allow us to do a biome-to-biome comparison; Extended Data Fig. 3). In grasslands, our estimation of significant negative ΔSOC_E is comparable to the estimation of field experiments. Forest ecosystems on average are less vulnerable to EDM than grasslands, and our estimation is not significantly different from experimental estimations, which, however, show much larger uncertainties (Extended Data Fig. 3). In shrublands, we estimate comparable negative ΔSOC_E between grasslands and shrublands, but field observations are generally positive albeit insignificant. Averaging across the globe, field manipulative experiments observed smaller response of SOC to the same level of EDM changes (Extended Data

https://doi.org/10.1038/s41558-023-01874-3

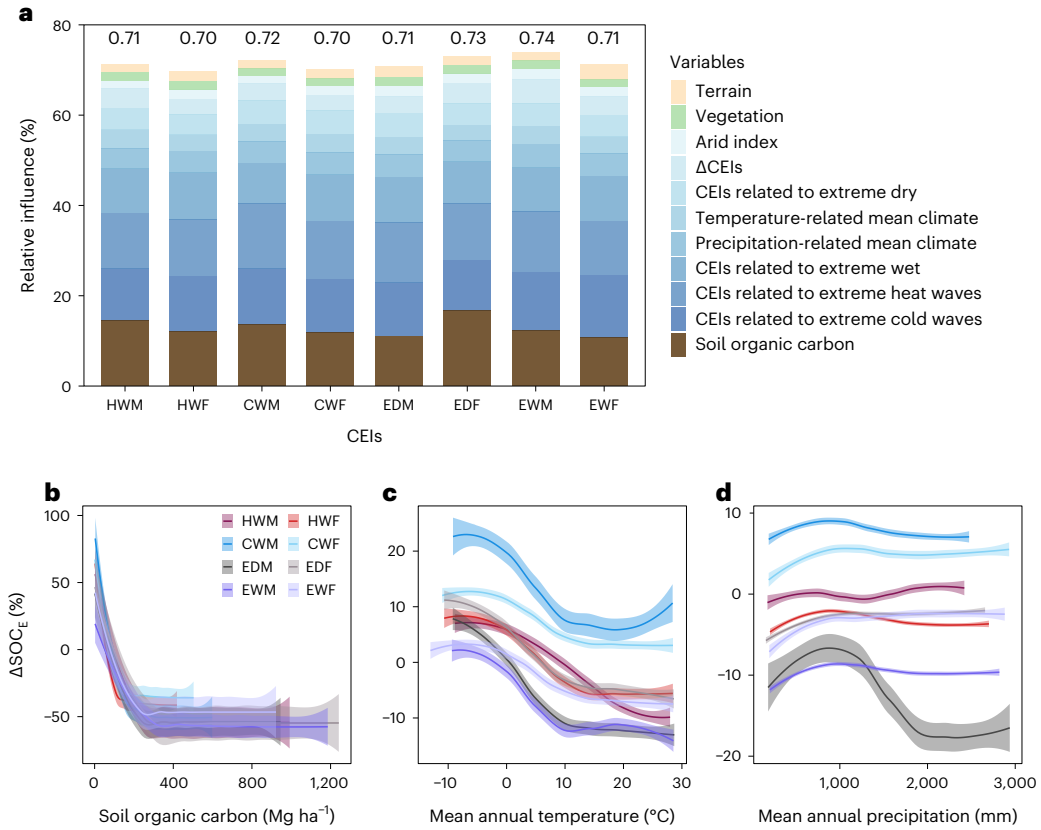

Fig. 4 | Influences of environmental variables on SOC changes attributed to climate extreme shifts under warming. a, The relative influences are estimated using a machine learning-based statistic model (that is, random forest) taking into account nonlinear relationships. Numbers above the bars show the determination coefficients of the model for explaining the influence of the corresponding CEI. **b**–**d**, Partial dependence of ΔSOC_E on SOC stock (**b**), mean annual temperature (**c**) and precipitation (**d**). Detailed descriptions of individual CEIs and predictor variables are shown in Supplementary Tables 1 and 2, respectively.

Fig. 3). In the short time (for example, the duration of field experiments ranges from 1 to 13 years; ref. 18), drought usually induces immediate reduction of soil respiration, yet carbon inputs do not change much and thereby exerting limited effect on net SOC balance. In the long term, however, EDM increase may substantially decrease carbon inputs to soil through increased plant mortality and decreased vegetation productivity[34], which cannot be fully captured by relative short manipulative experiments.

Drivers of the responses of SOC to climate extremes

We trained a machine learning model—random forest (RF)—to explore controls over the variance of ΔSOC_E for the eight CEIs indicating the magnitude and frequency of heatwave, cold waves, extreme dry and wet events (Methods). For all eight CEIs, the RF model driven by climatic attributes related to mean and extreme climate conditions, soil properties, vegetation characteristics and topographic attributes explains >70% of the variance of ΔSOC_E (Fig. 4a and Extended Data Fig. 4). Baseline SOC level is the most important individual predictor and alone explains 15–18% of the variance of ΔSOC_E. For all eight CEIs, ΔSOC_E is negatively associated with baseline SOC levels and remains constant until SOC reaches a threshold of ~300 Mg C ha^{-1} (Fig. 4b). However, it should be acknowledged that baseline SOC itself should not be explained as the driving force of SOC dynamics[35]. We find that those carbon-rich soils mainly distribute nearby or in wetlands including peatland and coastal areas and another small fraction in tundra, which has relatively low temperature (Extended Data Fig. 5). In these systems, particulate organic carbon (POC) usually dominates SOC[36] and is more sensitive to climate change than other SOC components such as mineral-associated organic carbon[37], which may result in general strong response of SOC to climate change. However, POC has much higher C:N ratio than mineral-associated organic carbon[36]; its decomposition is strongly dependent of nutrient availability, which would limit its response to climate change when POC is quite high[38]. In addition, under climate change, particularly warming and drought-relevant events, wetland soils may become less anaerobic and suffer from subsidence[39], thereby altering SOC density and the estimation of SOC changes based on soil depth. Overall, wetlands involve complex interactive responses of aboveground (for example, vegetation shift) and belowground process (for example, oxidation, subsidence, shift of anaerobic and aerobic conditions) to climate change, which may play a vital role in determining wetland SOC balance[40].

Baseline climatic attributes together contribute the largest fraction (42–51%) to the explained variance of ΔSOC_E for all CEIs (Fig. 4a), and their influence is obviously nonlinear (Fig. 4 and Extended Data Fig. 6). Mean annual temperature negatively influences ΔSOC_E (Fig. 4c), whereas the influence of mean annual precipitation is marginal and much weaker except for extreme dry magnitude (Fig. 4d vs 4a), demonstrating that SOC is generally more vulnerable to extreme dry events in warmer and wetter regions. However, extreme climate conditions together are more important than mean climate, suggesting that baseline climate extreme conditions play a vital role in determining the effect of future climate extreme shifts on SOC. Especially, we found strong dependency of ΔSOC_E induced by a typical CEI on the corresponding baseline CEI (Extended Data Fig. 6). For example, if the baseline magnitude of EDM is already high, more extreme conditions

https://doi.org/10.1038/s41558-023-01874-3

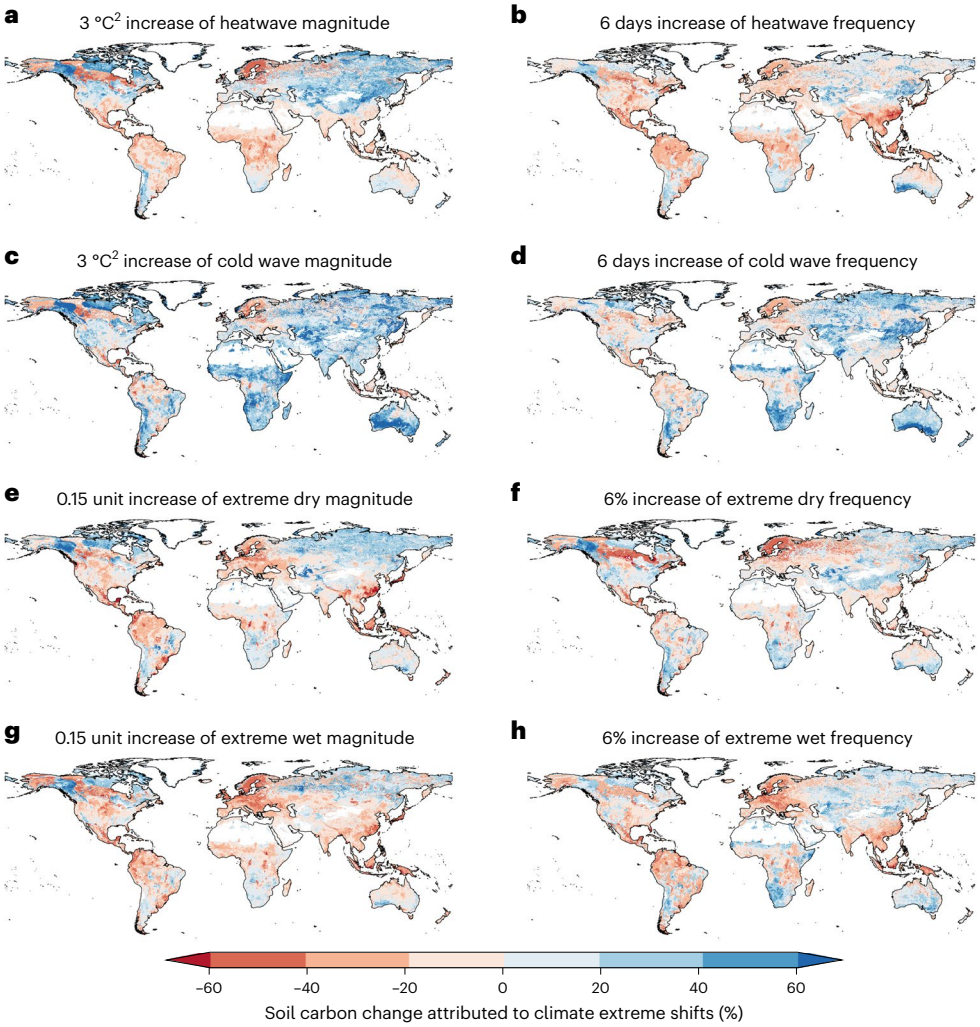

Fig. 5 | Global spatial pattern of changes in soil organic carbon attributed to climate extreme shifts under a warmer and more extreme climate. ΔSOC_E is defined as the difference between percentage responses of SOC to W + E and that to W, which can also be explained as the additional changes in SOC induced by climate extremes. **a**–**h**, Eight climate extremes including heat wave magnitude (**a**) and frequency (**b**), cold wave magnitude (**c**) and frequency (**d**), extreme dry magnitude (**e**) and frequency (**f**), extreme wet magnitude (**g**) and frequency (**h**).

have a smaller effect on ΔSOC_E. The positive effect of decreasing cold wave magnitude (CWM) is much stronger in regions with higher baseline CWM.

Although our study does not explicitly assess the underlying mechanisms, biome-specific responses to climate extremes are probably associated with interactive effects of water and energy on both carbon inputs and outputs over space and time. Energy-limited systems (for example, boreal forests and tundra) would be more sensitive to temperature-related extremes. In boreal forests, for example, the reduction of extreme cold events substantially stimulates plant growth superseding enhanced SOC decomposition[41,42], resulting in net SOC gains[43,44]. This is corroborated with the positive effects of shortening of cold spells, lengthening of warm spells and other temperature-related extremes (Fig. 3 and Extended Data Fig. 2). In tundra, reduction of energy limitation may accelerate permafrost thaw and thereby stimulate microbial growth and SOC decomposition[32,33]. Water-limited systems (for example, grasslands and savannahs) would be more sensitive to extremes that alter seasonal precipitation patterns or worsen/loosen water limitation. Additionally, the characteristics of vegetations (for example, canopy height, litter layer, rooting depth) would also mediate how ecosystems respond to climate extremes. Woody systems (for example, forests and shrublands) may be more tolerant to extreme wet conditions than herbaceous systems (for example, grasslands and croplands)[45] and the existence of an organic layer would increase soil water holding capacity and prevent or weaken the loss of particulate and dissolved organic carbon via erosion or runoff[46]. Indeed, our results show that extreme wet frequency shows positive effects in forests and shrubland ecosystems but negative effects in grasslands and croplands (Extended Data Fig. 2). Overall, climate extreme shifts may alter water–energy interactions depending on local climatic conditions, which then change plant performance and SOC decomposition and stabilization processes such as shifts in microbial community functioning and substrate utilization strategies[17,47] and thereby induce diverse effects of climate extremes across ecosystems.

Global pattern of SOC responses to climate extremes

We apply the cross-validated RF models (Extended Data Fig. 4) to map ΔSOC_E induced by changes in the eight CEIs (that is, the magnitude and frequency of heatwave, cold wave, extreme dry and extreme wet) across the globe (Fig. 5 and Extended Data Fig. 7) and its uncertainty (Extended Data Figs. 8 and 9). Global average additional ΔSOC_E is estimated to be −139 ± 7.1, −98 ± 4.5, −27 ± 6.1, −4.5 ± 6.3, −125 ± 5.8, −106 ± 5.2, −130 ± 5.8, −160 ± 5.8 Pg (mean ± standard error) for the eight CEIs, respectively

(Supplementary Table 3). There are hotspots of SOC response, albeit the global average SOC change is small under some extremes (Fig. 5 and Extended Data Fig. 10). For example, a 0.15 unit increase in drought magnitude (which is equivalent to a 40% increase of its global average) only leads to additional <1% reduction of global SOC (Extended Data Fig. 10e) but induces 50 Pg SOC reduction in tropical and subtropical regions, North America and Europe (Supplementary Table 3) and increases SOC in many high latitudinal regions, especially in Siberia (Fig. 5e and Extended Data Fig. 7e). Six-day increase of annual heatwave frequency results in 6% additional SOC reduction averaging across the globe (Extended Data Fig. 10b). This reduction is mainly in tropical and subtropical regions, North America and northern Europe (Fig. 5b and Extended Data Fig. 7b). A 6% increase of drought frequency does not significantly alter global SOC (Extended Data Fig. 10f) but leads to substantial additional reduction in northern European and North American wetlands (Fig. 5f).

More intense (0.15 unit increase in magnitude) and frequent (6% increase in frequency) precipitation extremes result in SOC reduction by 7% and 2%, respectively, across the globe (Extended Data Fig. 10g,h). The most vulnerable regions to extreme precipitation are Europe, North America and some tropical and subtropical regions (Fig. 5g,h). However, more frequent heavy precipitation can offset warming-induced SOC reduction in dry and semi-arid regions, such as central Asia, Australia, South Africa and the Sahel region (Fig. 5h). Fewer cold waves significantly decrease SOC reduction (that is, positive ΔSOC_E) in most regions of the globe (Fig. 5c,d and Extended Data Fig. 7c,d). Our results indicate that there are distinct hotspots in ΔSOC_E depending on the type of climate extreme. However, there are regions where SOC is vulnerable to all climate extremes. These regions mainly locate in Europe, southeast Asia, North America and the Amazon. Unfortunately, these regions are also hotspots experiencing more frequent and intense climate extremes[48,49].

Limitations and uncertainties

The space-for-time substitution approach has some limitations and uncertainties, for example, without considering other global change factors (for example, nitrogen deposition and wildfire) and the steady state assumption[21]. However, the impacts of these factors are more difficult to quantify as they usually exert much larger spatial variability (for example, wildfire), and the relevant data are also relatively limited. Croplands are the land-use type greatly affected by human activities in terms of both cultivation length (from years to millennia) and land management. Thus, SOC stocks are unlikely to be under steady state in croplands. However, excluding soil profiles from croplands, the estimated response of SOC to climate extremes did not apparently change (Supplementary Fig. 3), suggesting that steady state assumption would have little effect on our SOC change projection under projected climate extremes. A number of other sensitivity analyses have also demonstrated the robustness of the approach (Methods and Supplementary Figs. 4–6). Another limitation is that only two compound events involving two types of climate extreme were assessed. The natural environment may experience multiple compound events over different timescales. We acknowledge that more analyses focusing on compound events and their influence are needed[50]. However, potential interconnections among different types of climate extreme involved in compound events need to be clearly defined and quantified, which itself remains a challenge[26].

Conclusions

We used a novel approach to infer SOC changes induced by a warmer climate with more climate extremes. Our approach implicitly takes long-term transition of ecosystems into account and quantifies the SOC difference between steady states under contrasting climate conditions, which is otherwise impossible by conducting field experiments or modelling without explicit understanding of the underlying mechanisms. The results reveal distinct (positive, neutral or negative) responses of SOC to the shifts of different types of climate extreme. On a global scale, on average, most climate extremes may exacerbate SOC loss under future climate. Among ecosystems, however, the magnitude and direction of the effects are ecosystem dependent. Temperate grasslands, croplands and tropical/subtropical forests are sensitive to most climate extremes under warming. Tundra showed the strongest response to a series of climate extremes compared with other ecosystems. Studies focusing on the impacts of climate extremes on tundra SOC and carbon-rich soils (for example, wetland soil) are urgently needed. Our results and mapping provide a benchmark for identifying biome-specific critical climate extremes and sensitive areas of SOC changes as a result of climate extremes. These results demonstrate that climate extremes play a key role in determining SOC balance under climate change probably via modulating local water–energy interactions, thereby carbon inputs and SOC decomposition and stabilization processes, which must be considered in Earth system models and related climate policies, to gain a more reliable prediction for SOC dynamics in response to climate change.

Online content

Any methods, additional references, Nature Portfolio reporting summaries, source data, extended data, supplementary information, acknowledgements, peer review information; details of author contributions and competing interests; and statements of data and code availability are available at https://doi.org/10.1038/s41558-023-01874-3.

References

1. Seneviratne., S. I. et al. in *Managing the Risks of Extreme Events and Disasters to Advance Climate Change Adaptation* (eds Field, C. B. et al.) 109–230 (Cambridge Univ. Press, 2012).
2. Reichstein, M. et al. Climate extremes and the carbon cycle. *Nature* **500**, 287–295 (2013).
3. Frank, D. et al. Effects of climate extremes on the terrestrial carbon cycle: concepts, processes and potential future impacts. *Glob. Change Biol.* **21**, 2861–2880 (2015).
4. Gampe, D. et al. Increasing impact of warm droughts on northern ecosystem productivity over recent decades. *Nat. Clim. Change* **11**, 772–779 (2021).
5. Ciais, P. et al. Europe-wide reduction in primary productivity caused by the heat and drought in 2003. *Nature* **437**, 529–533 (2005).
6. Zscheischler, J., Mahecha, M. D., Harmeling, S. & Reichstein, M. Detection and attribution of large spatiotemporal extreme events in Earth observation data. *Ecol. Inf.* **15**, 66–73 (2013).
7. Sippel, S. et al. Drought, heat, and the carbon cycle: a review. *Curr. Clim. Change Rep.* **4**, 266–286 (2018).
8. Friedlingstein, P. et al. Global carbon budget 2021. *Earth Syst. Sci. Data* **14**, 1917–2005 (2022).
9. Crowther, T. W. et al. Quantifying global soil carbon losses in response to warming. *Nature* **540**, 104–108 (2016).
10. Xiao, L. et al. Younger carbon dominates global soil carbon efflux. *Glob. Change Biol.* **28**, 5587–5599 (2022).
11. Smith, M. D., Knapp, A. K. & Collins, S. L. A framework for assessing ecosystem dynamics in response to chronic resource alterations induced by global change. *Ecology* **90**, 3279–3289 (2009).
12. Sippel, S., Zscheischler, J. & Reichstein, M. Ecosystem impacts of climate extremes crucially depend on the timing. *Proc. Natl Acad. Sci. USA* **113**, 5768–5770 (2016).
13. Lugato, E. et al. Soil erosion is unlikely to drive a future carbon sink in Europe. *Sci. Adv.* **4**, eaau3523 (2018).
14. Van Oost, K. et al. The impact of agricultural soil erosion on the global carbon cycle. *Science* **318**, 626–629 (2007).

15. Anderegg, W. R. et al. Pervasive drought legacies in forest ecosystems and their implications for carbon cycle models. *Science* **349**, 528–532 (2015).
16. Anjileli, H. et al. Extreme heat events heighten soil respiration. *Sci. Rep.* **11**, 6632 (2021).
17. Bardgett, R. D. & Caruso, T. Soil microbial community responses to climate extremes: resistance, resilience and transitions to alternative states. *Philos. Trans. R. Soc. Lond. B* **375**, 20190112 (2020).
18. Deng, L. et al. Drought effects on soil carbon and nitrogen dynamics in global natural ecosystems. *Earth Sci. Rev.* **214**, 103501 (2021).
19. Diffenbaugh, N. S. et al. Quantifying the influence of global warming on unprecedented extreme climate events. *Proc. Natl Acad. Sci. USA* **114**, 4881–4886 (2017).
20. Fischer, E. M., Sippel, S. & Knutti, R. Increasing probability of record-shattering climate extremes. *Nat. Clim. Change* **11**, 689–695 (2021).
21. Wang, M. et al. Global soil profiles indicate depth-dependent soil carbon losses under a warmer climate. *Nat. Commun.* **13**, 5514 (2022).
22. Karl, T. R., Nicholls, N. & Ghazi, A. in *Weather and Climate Extremes: Changes, Variations and a Perspective from the Insurance Industry* (eds Karl, T. R. et al.) 3–7 (Springer Netherlands, 1999).
23. Mistry, M. A high-resolution global gridded historical dataset of climate extreme indices. *Data* **4**, 41 (2019).
24. Karl, T. R., Nicholls, N. & Ghazi, A. Clivar/GCOS/WMO workshop on indices and indicators for climate extremes workshop summary. *Weather Clim. Extremes* **42**, 3–7 (1999).
25. Kim, Y.-H., Min, S.-K., Zhang, X., Sillmann, J. & Sandstad, M. Evaluation of the CMIP6 multi-model ensemble for climate extreme indices. *Weather. Clim. Extremes* **29**, 100269 (2020).
26. Zscheischler, J. et al. Future climate risk from compound events. *Nat. Clim. Change* **8**, 469–477 (2018).
27. Bardgett, R. D. & Caruso, T. Soil microbial community responses to climate extremes: resistance, resilience and transitions to alternative states. *Philos. Trans. R. Soc. B* **375**, 20190112 (2020).
28. Bennett, A. C. et al. Resistance of African tropical forests to an extreme climate anomaly. *Proc. Natl Acad. Sci. USA* **118**, e2003169118 (2021).
29. Zhao, M. & Running, S. W. Drought-induced reduction in global terrestrial net primary production from 2000 through 2009. *Science* **329**, 940–943 (2010).
30. Tao, F. et al. Microbial carbon use efficiency promotes global soil carbon storage. *Nature* **618**, 981–985 (2023).
31. Eckardt, N. A. et al. Climate change challenges, plant science solutions. *Plant Cell* **35**, 24–66 (2023).
32. Xue, K. et al. Tundra soil carbon is vulnerable to rapid microbial decomposition under climate warming. *Nat. Clim. Change* **6**, 595–600 (2016).
33. Plaza, C. et al. Direct observation of permafrost degradation and rapid soil carbon loss in tundra. *Nat. Geosci.* **12**, 627–631 (2019).
34. Liu, Q. et al. Drought-induced increase in tree mortality and corresponding decrease in the carbon sink capacity of Canada's boreal forests from 1970 to 2020. *Glob. Change Biol.* **29**, 2274–2285 (2023).
35. Slessarev, E. W. et al. Initial soil organic carbon stocks govern changes in soil carbon: reality or artifact? *Glob. Change Biol.* **29**, 1239–1247 (2023).
36. Cotrufo, M. F., Ranalli, M. G., Haddix, M. L., Six, J. & Lugato, E. Soil carbon storage informed by particulate and mineral-associated organic matter. *Nat. Geosci.* **12**, 989–994 (2019).
37. Lugato, E., Lavallee, J. M., Haddix, M. L., Panagos, P. & Cotrufo, M. F. Different climate sensitivity of particulate and mineral-associated soil organic matter. *Nat. Geosci.* **14**, 295–300 (2021).
38. Du, E. et al. Global patterns of terrestrial nitrogen and phosphorus limitation. *Nat. Geosci.* **13**, 221–226 (2020).
39. Wang, H., Richardson, C. J. & Ho, M. Dual controls on carbon loss during drought in peatlands. *Nat. Clim. Change* **5**, 584–587 (2015).
40. Bao, T., Jia, G. & Xu, X. Weakening greenhouse gas sink of pristine wetlands under warming. *Nat. Clim. Change* **13**, 462–469 (2023).
41. Gauthier, S., Bernier, P., Kuuluvainen, T., Shvidenko, A. Z. & Schepaschenko, D. G. Boreal forest health and global change. *Science* **349**, 819–822 (2015).
42. Wang, J., Taylor, A. R. & D'Orangeville, L. Warming-induced tree growth may help offset increasing disturbance across the Canadian boreal forest. *Proc. Natl Acad. Sci. USA* **120**, e2212780120 (2023).
43. Jarvis, P. & Linder, S. Constraints to growth of boreal forests. *Nature* **405**, 904–905 (2000).
44. Lim, H. et al. Boreal forest biomass accumulation is not increased by two decades of soil warming. *Nat. Clim. Change* **9**, 49–52 (2018).
45. Wang, P., Huang, K. & Hu, S. Distinct fine-root responses to precipitation changes in herbaceous and woody plants: a meta-analysis. *New Phytol.* **225**, 1491–1499 (2020).
46. Vereecken, H. et al. Soil hydrology in the Earth system. *Nat. Rev. Earth Environ.* **3**, 573–587 (2022).
47. García-Palacios, P. et al. Evidence for large microbial-mediated losses of soil carbon under anthropogenic warming. *Nat. Rev. Earth Environ.* **2**, 507–517 (2021).
48. Ridder, N. N. et al. Global hotspots for the occurrence of compound events. *Nat. Commun.* **11**, 5956 (2020).
49. Xu, L., Wang, A., Wang, D. & Wang, H. Hot spots of climate extremes in the future. *J. Geophys Res. Atmos.* **124**, 3035–3049 (2019).
50. Tschumi, E. & Zscheischler, J. Countrywide climate features during recorded climate-related disasters. *Climatic Change* **158**, 593–609 (2020).

Methods

Data sources

We used the same global dataset of SOC stock (Mg C ha^{-1}) as ref. 23. The dataset includes 110,695 SOC measurements in the 0–30 cm soil layer depth compiled into the World Soil Information Service (WoSIS) snapshot of 2019, which was collated and managed by the WoSIS[51]. The dataset includes the snapshot of 2019. Another 2,778 measurements for the 0–30 cm soil layer from permafrost-affected regions[52] were also included in the dataset. In brief, the data were quality-assessed and standardized using consistent procedures. The dataset covers nine major biome groups (Supplementary Fig. 1) under various climate conditions across the globe. At the locations of SOC measurements, mean annual temperature (MAT) ranges from −20.0 to 30.7 °C and mean annual precipitation (MAP) from 0 to 6,674 mm.

MAT and MAP at each soil location were extracted from WorldClim version 2 (ref. 53), which is a global mapping product at the resolution of 0.0083° × 0.0083° using monthly temperature and precipitation recorded for the period 1970–2000. Soil profiles in the same 0.0083° grid (that is, ~1 km^2) share the same MAT and MAP. The WWF map of terrestrial ecoregions of the world[54] was used to extract the biome type at each soil profile. The MODIS land-cover map[55] at the same resolution of WorldClim was used to identify that if the soil profile is located in a cultivated land (that is, cropland or cropland/natural vegetation mosaic). A global landform spatial layer was obtained from Global Landform Classification[56] (https://esdac.jrc.ec.europa.eu/content/global-landform-classification) to identify the landform at each soil location. Global terrestrial lands were divided into three general landform types: plains including lowlands, plateaus and mountains including hills. A global spatial layer of the 12 soil orders defined by the U.S. Department of Agriculture (https://www.nrcs.usda.gov/resources/guides-and-instructions/soil-taxonomy) were used to distinguish the soil type for each soil profile.

Climate extremes

At the location of each soil profile, 25 climate extreme indices (CEIs) defined by the expert team on Climate Change Detection and Indices[57] were extracted from a high-resolution historical dataset of climate extreme indices[23] (that is, a gridded mapping product at the resolution of 0.25° × 0.25°, which is equivalent to ~25 km at the equator). In brief, the average CEIs were calculated based on sub-daily temperature and precipitation observations during the period 1970–2016 using the climate data managed by the Global Land Data Assimilation System[58], representing baseline climate extreme conditions such as the intensity and frequency of heatwaves, drought and heavy precipitation. Soil profiles located in the same 0.25° × 0.25° grid (that is, ~25 km × ~25 km) share the same CEIs. A detailed description of CEIs is listed in Supplementary Table 1.

In addition, another eight indices indicating the magnitude and frequency of heatwave, cold waves, extreme dry and wet events (Supplementary Table 1) were also obtained from this global mapping product of CEIs (Supplementary Fig. 2)[23]. A heatwave event is defined as consecutive 3 or more days with a positive value of the excess heat factor[59]. The magnitude and frequency of heatwaves (HWM and HWF) are the average temperature across all individual heatwave events and the total number of days that contribute to all heatwave events every year, respectively. The cold wave event is identified by the excess cold factor[60] with a negative value for consecutive 3 or more days. The mean magnitude and frequency of cold wave (CWM and CWF) are the mean temperature and number of days of all cold wave events, respectively. The standardized precipitation index (SPI) at the temporal resolution of 3 months (ref. 61) in this global historical dataset of CEIs[23] was used to identify extreme dry and wet events. An extreme dry event (that is, drought) was identified if SPI ≤ −1, and an extreme wet event was identified if SPI > 1 (refs. 62,63). Then, the intensities of every extreme dry and wet events were calculated as the average of the difference between SPI in event duration and event thresholds. The average magnitude of extreme dry and wet event (EDM and EWM) is the average value of intensity of individual events during the period 1970–2016. Their average frequency was calculated as the percentage of total extreme dry and wet (EDF and EWF) months in total months during the period 1970–2016.

Space-for-time substitution-based grouping

Taking advantage of the big dataset of more than 100,000 soil profiles, we adopted an approach combining space-for-time substitution with meta-analysis techniques[21] to estimate the role of climate extremes in regulating the response of SOC to warming. This approach controls the effects of other confounding variables that play an important role in regulating SOC stocks and their spatial distribution such as soil type and landform and precipitation and its seasonality and conducts assessment based on grouped data distinguished by the intensity and/or frequency of climate extremes of interest.

The approach has been explicitly described in ref. 21 and applied to estimate the response of whole-soil profile SOC dynamics to warming without considering climate extremes[21]. In this study, we quantify the influences of climate extremes on SOC dynamics under climate warming by comparing SOC changes under two general climate scenarios (Fig. 1): warming alone (W) and warming with changes in climate extremes represented by the 33 CEIs (W + E). For each CEI, the estimated response under W + E was compared to that under W. In addition, because there are no consistent estimations on the magnitude of the changes of climate extremes[1], a potential change gradient with five levels is assigned to each CEI (ΔCEI; Supplementary Table 1). For this reason, there are a total of 165 comparisons (that is, 33 CEIs × five change levels). For each CEI, in detail, the estimation starts from a soil profile randomly selected from the 113,013 soil profiles. This soil profile is used as a criterion to select a group of soils sharing the same MAT, CEI, MAP, precipitation seasonality, landform and soil type. This group is called ambient group (A group).

Then, another two groups (that is, W and W + E groups) are selected according to the same selection criterion as the A group, except that MAT in both W and W + E groups must be certain degrees higher (1.5 °C in this study, which is the global climate target[64]) than that in the A group to reflect warming, and CEI in the W + E group must be certain magnitude higher or lower (that is, the five change levels of CEI; Supplementary Table 1) than CEI in the A group to reflect shift of extreme climate. During the selection process, MAT, CEI and MAP of soil profiles (due to they are continuous variables) in the same group cannot be exactly the same, and tolerance values (τ, which defines the allowed maximum deviation of the variable of interest in the same group) of 0.5 °C and 25 mm were assigned for MAT and MAP, respectively. To make the estimation more robust, these groups with less than five soil profiles are rejected. For each CEI, an empirical tolerance value has also been assigned by considering its distribution across the globe (Supplementary Table 1). These tolerance values are different among the CEIs. By conducting this selection and grouping, we obtained triples including A, W and W + E groups. With the replacement of the selected profile within the triple, the same random sampling, selection and grouping procedure have been applied until the number of triples is large enough to obtain robust estimation of response ratio (Supplementary Fig. 3). At last, we obtain a set of triples with the same warming and climate extreme change levels under different environmental conditions (that is, ambient MAT and CEI, MAP, precipitation seasonality, soil type and landform).

Compound extreme events (that is, concurrent occurrence of multiple climate extremes) may be also more common in the future[26,65]. To estimate the response of SOC to compound climate extremes, several CEIs were simultaneously used to conduct the selection and grouping procedure to represent the occurrence of multiple events. Unfortunately, the data do not allow us to quantify the effects of all possible

compound events as more criteria have to be applied to the selection of triples for comparison, which will substantially shrink the number of triples, resulting in unreliable estimation. Here we quantified only the influence of shifts in two common compound events involving two individual events: heatwave + extreme dry and heatwave + extreme wet. The data allowed us to obtain only enough triples for the first two levels of changes of the two events. For this assessment, the similar sampling and selection processes for single events have been applied except that both CEIs were considered.

Estimation of the response of SOC to warming and climate extreme changes

Meta-analysis techniques were used to estimate the response of SOC to W and W + E by comparing SOC stock in the A group to that in the W and W + E groups, respectively. For *i*th selected triple (A, W and W + E), the logarithmic response ratios of SOC ($\ln R_i$) to W and W + E were calculated, respectively, as:

$$\ln R_{\mathrm{W},i} = \ln\left(\frac{\overline{\mathrm{SOC}_{\mathrm{W},i}}}{\overline{\mathrm{SOC}_{\mathrm{A},i}}}\right), \quad (1)$$

$$\ln R_{\mathrm{W+E},i} = \ln\left(\frac{\overline{\mathrm{SOC}_{\mathrm{W+E},i}}}{\overline{\mathrm{SOC}_{\mathrm{A},i}}}\right), \quad (2)$$

where $\overline{\mathrm{SOC}_{A,i}}$, $\overline{\mathrm{SOC}_{W,i}}$ and $\overline{\mathrm{SOC}_{W+E,i}}$ are the mean SOC stock in the *i*th A, W and W + E triples, respectively. The two response ratios enable us to estimate the response attributed to climate extreme changes ($\ln R_{\mathrm{E},i}$) as:

$$\ln R_{E,i} = \ln R_{\mathrm{W+E},i} - \ln R_{\mathrm{W},i} = \ln\left(\frac{\overline{\mathrm{SOC}_{\mathrm{W+E},i}}}{\overline{\mathrm{SOC}_{\mathrm{W},i}}}\right). \quad (3)$$

Then, the individual $\ln R_{\mathrm{E},i}$ values calculated for each triple were used to estimate a global mean response ratio ($\overline{\ln R_{\mathrm{E}}}$) by a weighted mixed-effects model using the *rma.av* function in package *metafor* in R 4.1.1. The weight (w) was calculated as the inverse of the sum of within- (v) and between-group (τ^2) variances in the same set of triples:

$$\overline{\ln R_{\mathrm{E}}} = \frac{\sum(\ln R_{\mathrm{E},i} \times w_i)}{\sum w_i}, \quad (4)$$

where $w_i = \frac{1}{v_i + \tau^2}$ is the weight for the $\ln R_{\mathrm{E},i}$ in the *i*th triple. The within-group variance (v) was calculated as:

$$v_i = \frac{S_e^2}{N_e X_e^2} + \frac{S_c^2}{N_c X_c^2}, \quad (5)$$

where S_e and S_c are the standard deviation of SOC in the A and W (or W + E) groups, respectively; X_e and X_c are the mean of SOC in the A and W (or W + E) groups, respectively; and N_e and N_c are the number of samples in the A and W (or W + E) groups, respectively. The between-group variance (τ^2) was estimated by restricted maximum likelihood. To assist interpretation, $\overline{\ln R_{\mathrm{E}}}$ was back transformed and reported as percentage change, that is, $(e^{\overline{\ln R_{\mathrm{E}}}} - 1) \times 100\%$. The back-transformed values were also used for subsequent data analyses.

Especially, the percentage change calculated from $\overline{\ln R_{\mathrm{E}}}$ was referred as the additional global percentage change induced by climate extremes under W + E ($\Delta\mathrm{SOC_E}$), that is, $\Delta\mathrm{SOC_E} = \left(e^{\overline{\ln R_{\mathrm{E}}}} - 1\right) \times 100\%$. A linear mixed-effects model treating ecosystem type as a random factor was fitted to assess the relationship between $\Delta\mathrm{SOC_E}$ and change levels of climate extremes using the *lmer* function in the lmerTest package in R 4.1.1.

Here we note that an implicit assumption underlying the space-for-time substitution approach is that critical land-surface processes, which substantially change the state or succession direction of studied triples (for example, volcano disruption-induced new soil formation and/or soil cultivation in one group but not in another group) are independent of space and time[66]. That is, soils in any typical triple were not and will not be differently influenced by other critical processes regulating SOC dynamics. In addition, the approach assumes that soils in the three groups of the same triple are at the same average succession stage (for example, steady state or similar succession direction). Croplands are subjected to substantial management interventions (for example, tillage, fertilizer application, irrigation), and these management interventions vary widely across space and over time. As such, croplands would not meet the assumption of steady state or similar succession direction, providing an opportunity to test the sensitivity of these assumptions on the results. To do so, we repeated all assessment by excluding soil profiles from croplands and compared the results with that including cropland soils (Supplementary Fig. 4). In addition, soils sampled at different times also may be at different stages; we repeated all assessment by excluding data measured before 1970 (Supplementary Fig. 5). In addition, we conducted a sensitivity test using a leave-out-out approach that sequentially removes one triple to calculate the grand means using the remaining data. For all CEIs, the results show that the grand means are not sensitive to any single triple (Supplementary Fig. 6).

Driver analysis and global mapping

Focusing on $\Delta\mathrm{SOC_E}$, we explained its variance by fitting a machine learning-based statistical model—random forest (RF) driven by 67 potential environmental variables (Supplementary Table 2), including mean and extreme climate conditions, soil properties, vegetation properties and terrain attributes. The RF model has an advantage of taking into account nonlinear and interactive relationships among predictors, providing a robust estimation of overall and individual importance of the assessed predictors. Before fitting the model, collinearity among the predictors is identified by variance inflation factor (VIF) using the *vif* function in the car package in R 4.1.1, and predictors with VIF of greater than 10 (28 out of the 67 variables) were removed from the model. Model hyperparameters (mtry, randomly selected predictors; splitrule, splitting rule; min.node.size, minimal node size) were optimized by using a tenfold cross-validated approach using the *train* function in the caret package in R 4.1.1. That is, 80% of data were used to train the RF model, and the remaining 20% data were used to validate the model (Extended Data Fig. 4). The best RF model was selected with the highest coefficient of determination (R^2).

The relative importance of each predictor was estimated by permutation variable importance measurements using the *varImp* function in package caret. Briefly, on the basis of the times a predictor was selected for splitting when growing a tree, the mean square error for every given regression tree with out-of-bag estimates is calculated. The change of model residuals due to that splitting represents the influence of the predictor. To compare the relative importance of individual predictors among CEIs, their influences were first normalized with the influence of the most important predictor and then multiplied by the corresponding model performance (that is, R^2). In addition, a partial dependence analysis was used to explore the partial dependence of $\Delta\mathrm{SOC_E}$ on CEI change gradients using the *partial* function in package *pdp* in R 4.1.1.

The RF model with the lowest rooted mean square error (RMSE) for predicting the effects of climate extremes on $\Delta\mathrm{SOC_E}$ was applied to the globe at the resolution of 0.25° × 0.25° using gridded data of model predictors (the Harmonized World Soil Database, i.e. the HSWD dataset[67], was used for baseline SOC level) to map the regulating effect of selected climate extreme shifts on SOC responses under 1.5 °C warming. This mapping was only demonstrated using the eight indices

representing the magnitude and frequency of extreme events with their median change levels (Supplementary Table 1). That is, the magnitude (HWM) and frequency of heatwaves (HWF) are increased by 3 °C and 6 days, respectively; the magnitude and frequency of both extreme dry (EDM) and wet (EWM) are increased 0.15 unit and 6%, respectively; the magnitude and frequency of cold wave (CWM and CWF) are decreased by 3 °C and 6 days, respectively. The uncertainty of the response was estimated as the standard error of individual predictions of 500 trees in the RF model (Extended Data Figs. 8 and 9).

Data availability

The 33 climate extreme indices can be accessed at https://doi.org/10.1594/PANGAEA.898014. Global mapping products generated in this study are publicly available and deposited to https://doi.org/10.6084/m9.figshare.22317202. Other data used in this study are the same to those used in ref. 21, which are publicly accessible. The coastline data in all maps can be gained from https://www.naturalearthdata.com/downloads/50m-physical-vectors/50m-coastline/.

Code availability

Code (R scripts)[68] used to assess the data and generate the results is deposited at https://doi.org/10.6084/m9.figshare.22317202.

References

51. Batjes, N. H., Ribeiro, E. & van Oostrum, A. Standardised soil profile data to support global mapping and modelling (WoSIS snapshot 2019). *Earth Syst. Sci. Data* **12**, 299–320 (2020).
52. Mishra, U. et al. Spatial heterogeneity and environmental predictors of permafrost region soil organic carbon stocks. *Sci. Adv.* **7**, eaaz5236 (2021).
53. Fick, S. E. & Hijmans, R. J. WorldClim 2: new 1-km spatial resolution climate surfaces for global land areas. *Int. J. Climatol.* **37**, 4302–4315 (2017).
54. Olson, D. M. et al. Terrestrial ecoregions of the world: a new map of life on Earth: a new global map of terrestrial ecoregions provides an innovative tool for conserving biodiversity. *Bioscience* **51**, 933–938 (2001).
55. Channan, S., Collins, K. & Emanuel, W. *Global Mosaics of the Standard MODIS Land Cover Type Data* (Univ. of Maryland & Pacific Northwest National Laboratory, 2014).
56. Meybeck, M., Green, P. & Vörösmarty, C. A new typology for mountains and other relief classes: an application to global continental water resources and population distribution. *Mt. Res. Dev.* **21**, 34–45 (2001).
57. Alexander, L. V. Global observed long-term changes in temperature and precipitation extremes: a review of progress and limitations in IPCC assessments and beyond. *Weather Clim. Extremes* **11**, 4–16 (2016).
58. Rodell, M. et al. The global land data assimilation system. *Bull. Am. Meteorol. Soc.* **85**, 381–394 (2004).
59. Alexander, L. V. & Perkins, S. E. On the measurement of heat waves. *J. Clim.* **26**, 4500–4517 (2013).
60. Sheridan, S. C. & Lee, C. C. Temporal trends in absolute and relative extreme temperature events across North America. *J Geophys. Res. Atmos.* **123**, 11889–11898 (2018).
61. Vicente-Serrano, S. M., Beguería, S. & López-Moreno, J. I. A multiscalar drought index sensitive to global warming: the standardized precipitation evapotranspiration index. *J. Clim.* **23**, 1696–1718 (2010).
62. Schwalm, C. R. et al. Global patterns of drought recovery. *Nature* **548**, 202–205 (2017).
63. Chen, H., Wang, S., Zhu, J. & Zhang, B. Projected changes in abrupt shifts between dry and wet extremes over China through an ensemble of regional climate model simulations. *J. Geophys. Res. Atmos.* **125**, e2020JD033894 (2020).
64. IPCC *Special Report on Global Warming of 1.5 °C* (eds Masson-Delmotte, V. et al.) (WMO, 2018).
65. Bevacqua, E., Zappa, G., Lehner, F. & Zscheischler, J. Precipitation trends determine future occurrences of compound hot–dry events. *Nat. Clim. Change* **12**, 350–355 (2022).
66. Strayer, D. et al. Long-term ecological studies: an illustrated account of their design, operation, and importance to ecology. *Occasional Publ. Inst. Ecosyst. Stud.* **2**, 1–38 (1986).
67. FAO, IIASA, ISRIC, ISS-CAS & JRC *Harmonized World Soil Database* version 1.2 (FAO & IIASA, 2012).
68. Wang, M. & Luo, Z. Changes in soil organic carbon in response to climate extremes under warming across globe biomes. *figshare* https://doi.org/10.6084/m9.figshare.22317202.v1 (2023).

Acknowledgements

This research has been financially supported by the National Natural Science Foundation of China (grant number 32241036, 32171639) and the National Key Research Program of the Ministry of Science and Technology of China (grant number 2021YFE0114500). Contributions of U.M. were supported through a US Department of Energy grant to the Sandia National Laboratories, which is a multi-mission laboratory managed and operated by National Technology and Engineering Solutions of Sandia LLC, a wholly owned subsidiary of Honeywell International Inc. for the US Department of Energy's National Nuclear Security Administration under contract DE-NA-0003525.

Author contributions

Z.L. conceived the study; M.W. and Z.L. led data assessment; Y.Y. and U.M. contributed to permafrost data; Z.L. and M.W. interpreted the results with the contribution of all authors; Z.L. and M.W. led the writing of the manuscript and all authors improved the manuscript.

Competing interests

The authors declare no competing interests.

Additional information

Extended data is available for this paper at https://doi.org/10.1038/s41558-023-01874-3.

Supplementary information The online version contains supplementary material available at https://doi.org/10.1038/s41558-023-01874-3.

Correspondence and requests for materials should be addressed to Zhongkui Luo.

Peer review information *Nature Climate Change* thanks Emanuele Lugato and the other, anonymous, reviewer(s) for their contribution to the peer review of this work.

https://doi.org/10.1038/s41558-023-01874-3

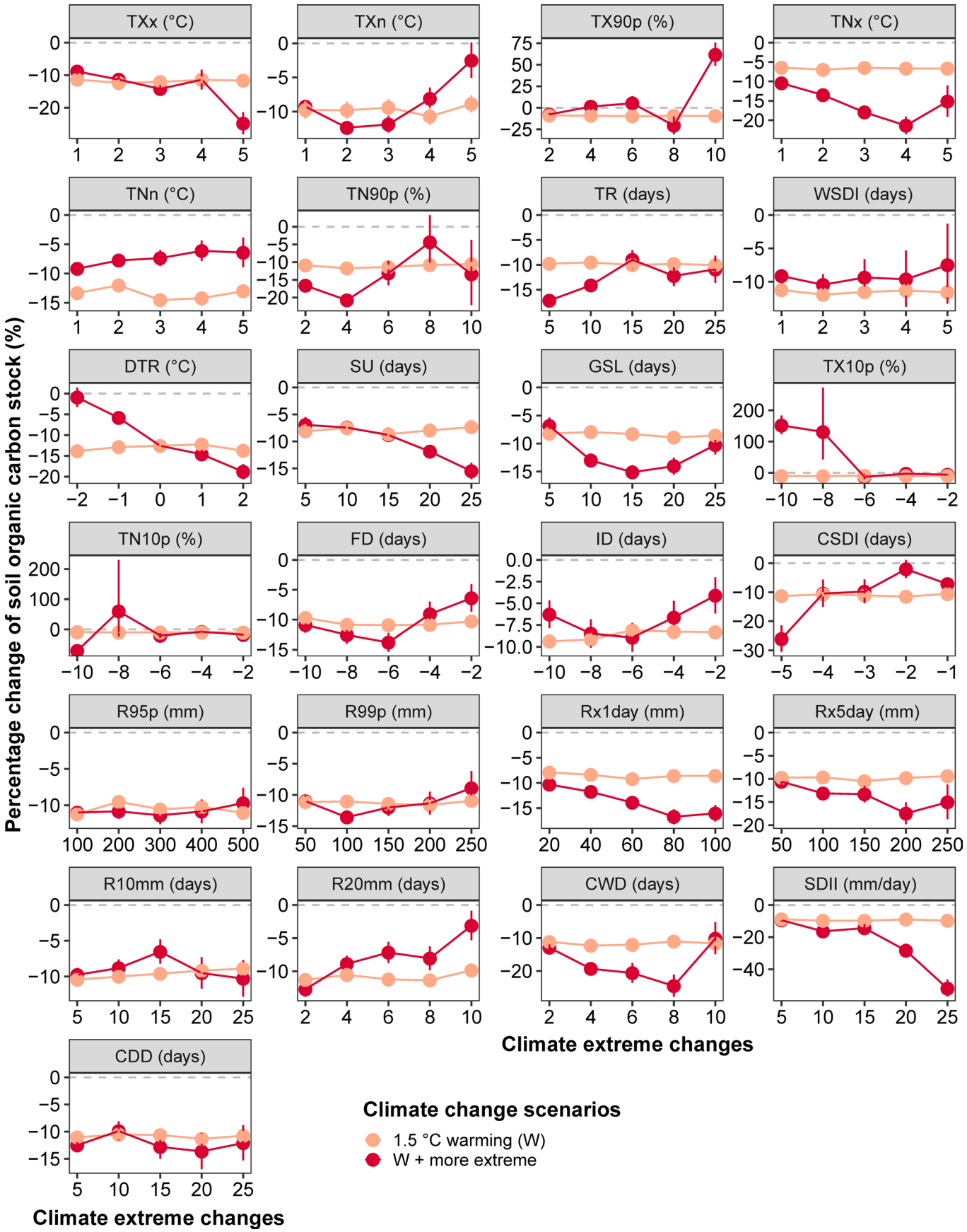

Extended Data Fig. 1 | The response of soil organic carbon to climate change scenarios. Error bars show 95% confidence interval, centred on the mean with the sample size shows Supplementary Data 1. Detailed descriptions of climate extreme indices (CEIs) and climate scenarios are shown in Supplementary Table 1.

https://doi.org/10.1038/s41558-023-01874-3

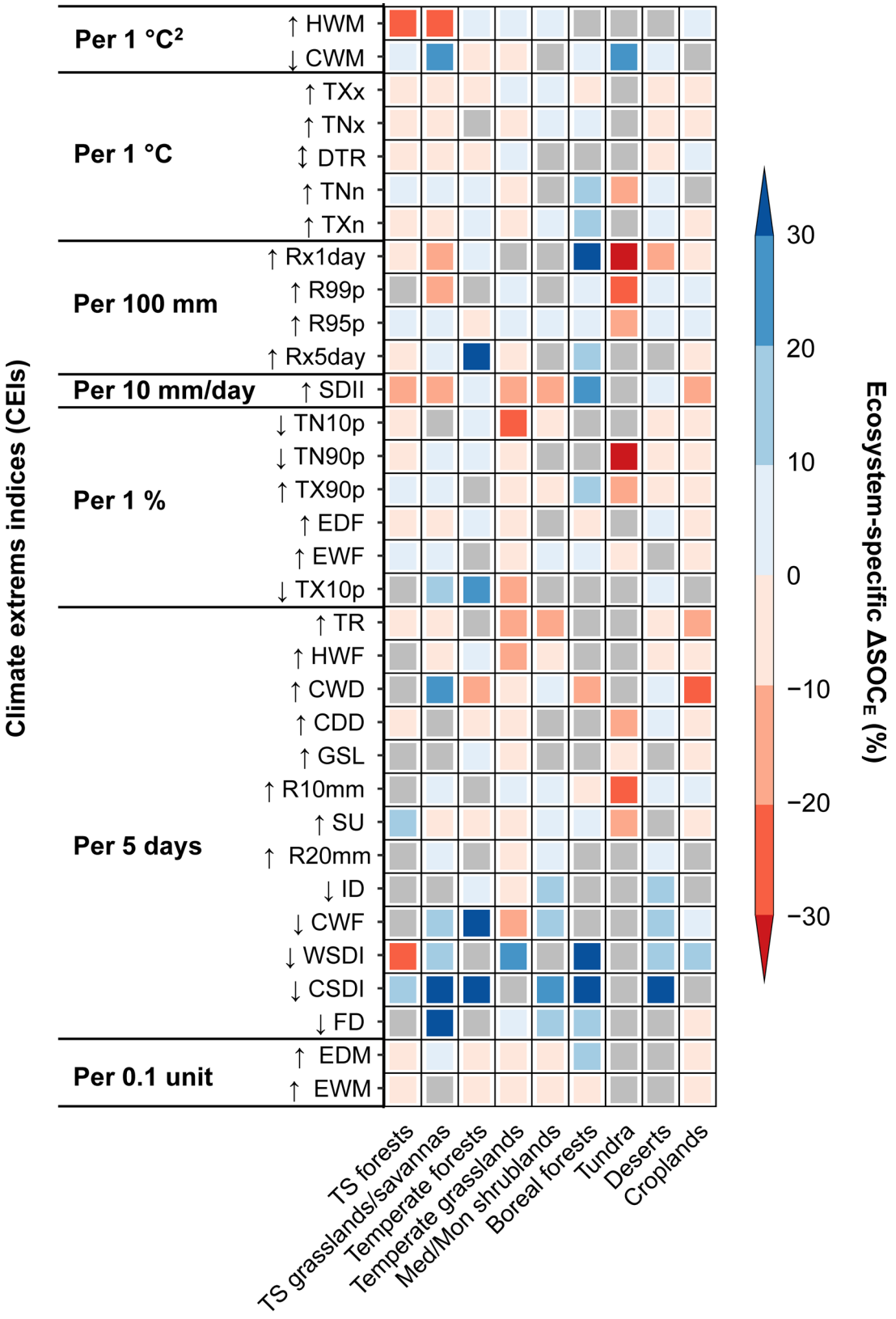

Extended Data Fig. 2 | The additional changes in soil organic carbon induced by climate extremes under a warmer and more extreme climate. The dependence of additional changes in soil organic carbon (ΔSOC_E) on the change levels of climate extremes under a warmer and more extreme climate. Grey grids indicate that the estimated dependence is statistically insignificant ($P > 0.05$). TS forests, tropical/subtropical forests; Med/Mon shrublands, Mediterranean/montane shrublands; TS grasslands/savannas, tropical/subtropical grasslands/savannas. Detailed descriptions of CEIs are shown in Supplementary Table 1.

https://doi.org/10.1038/s41558-023-01874-3

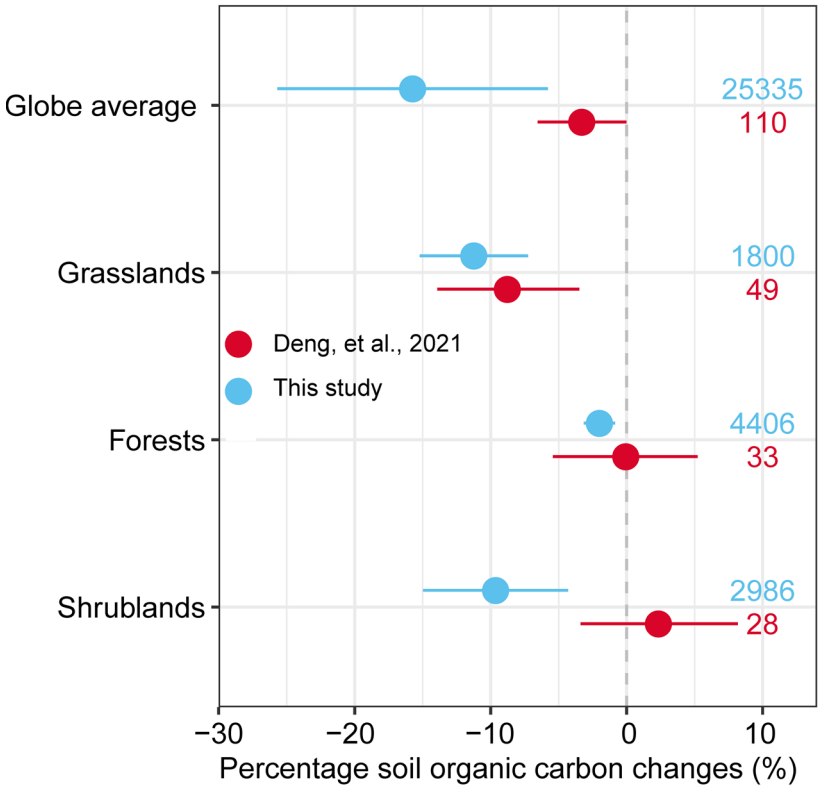

Extended Data Fig. 3 | The comparison of soil organic carbon changes induced by changes in extreme dry magnitude using our approach with file drought experimental results. Comparison of soil organic carbon changes induced by changes in extreme dry magnitude (EDM). Deng et al. (2021) synthesized the data from field experiments. Biomes are grouped into tundra, shrublands, grasslands, and forests. Dots with bars show the mean effect sizes with 95% confidence intervals, and numbers besides them are sample sizes used to calculate the mean effect size. The actual drought levels (that is, the reduction of precipitation) in field drought experiments were normalized to annual mean precipitation. The change level in our estimation which is close most to the experimental change level was targeted to conduct the comparison.

https://doi.org/10.1038/s41558-023-01874-3

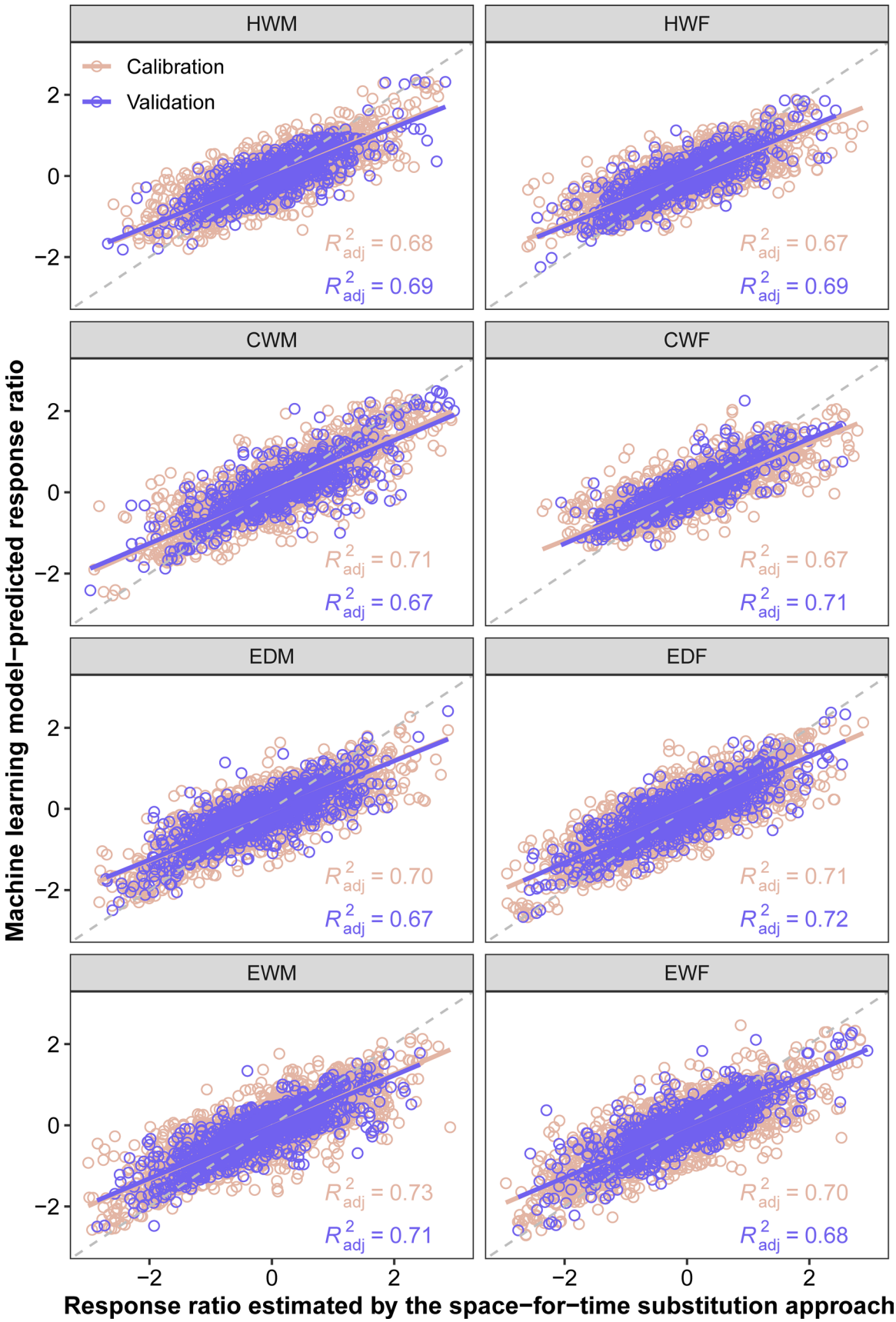

Extended Data Fig. 4 | The performance of random forest model. The performance of random forest model on predicting soil organic carbon responses attributed to eight climate extremes under a warmer and more extreme climate. Detailed descriptions of climate extreme indices (CEIs) are shown in Supplementary Table 1.

https://doi.org/10.1038/s41558-023-01874-3

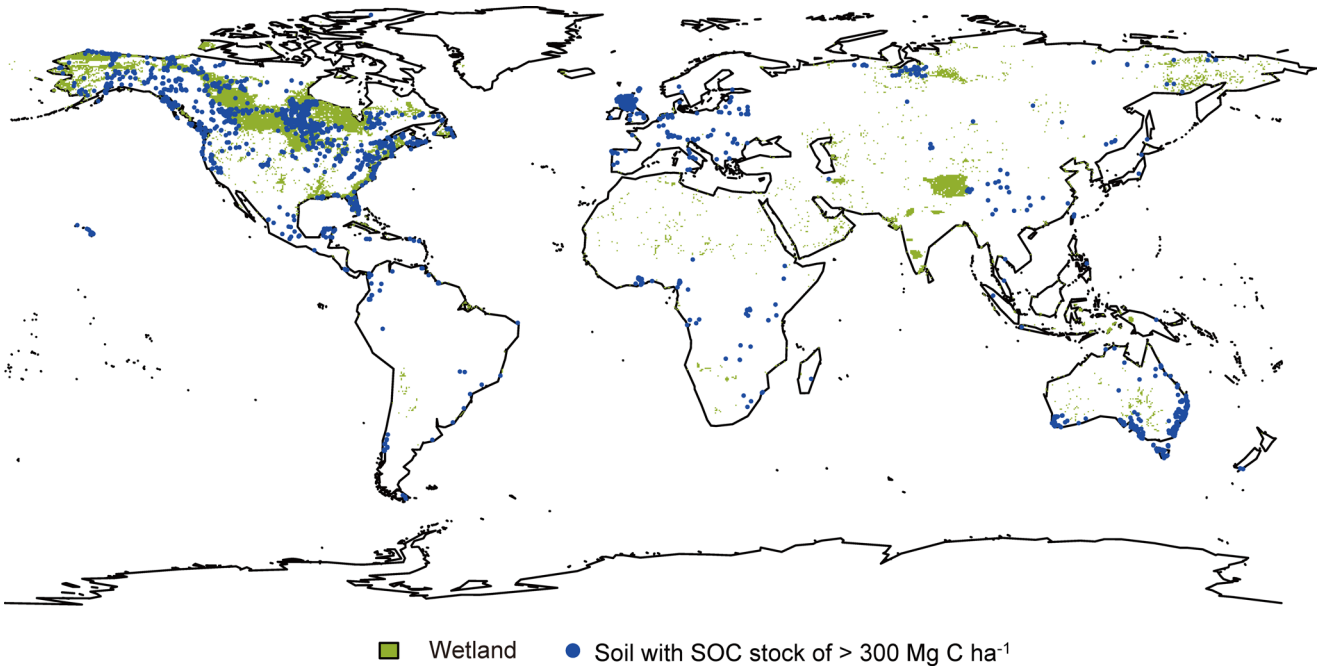

Extended Data Fig. 5 | The distribution of global wetlands and the location of soils with organic carbon stock of >300 Mg C ha^{-1} (0–30 cm) used in this study. The wetland map data is obtained from http://www.wwfus.org/science/data.cfm.

https://doi.org/10.1038/s41558-023-01874-3

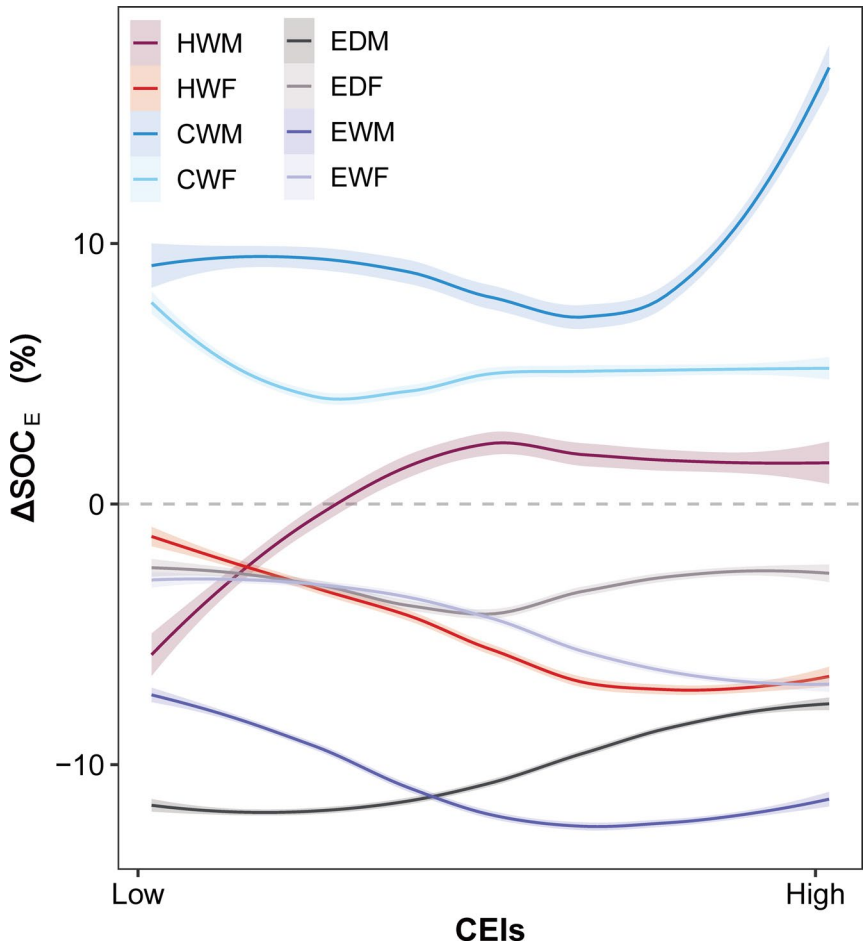

Extended Data Fig. 6 | The partial depended relationship of soil organic carbon changes with background climate extreme conditions. The relationship of soil organic carbon changes (that is, ΔSOC_E) with background climate extreme conditions. Partial dependence of ΔSOC_E induced by a typical CEI on corresponding background CEI. Detailed descriptions of the eight CEIs are shown in Supplementary Table 1.

https://doi.org/10.1038/s41558-023-01874-3

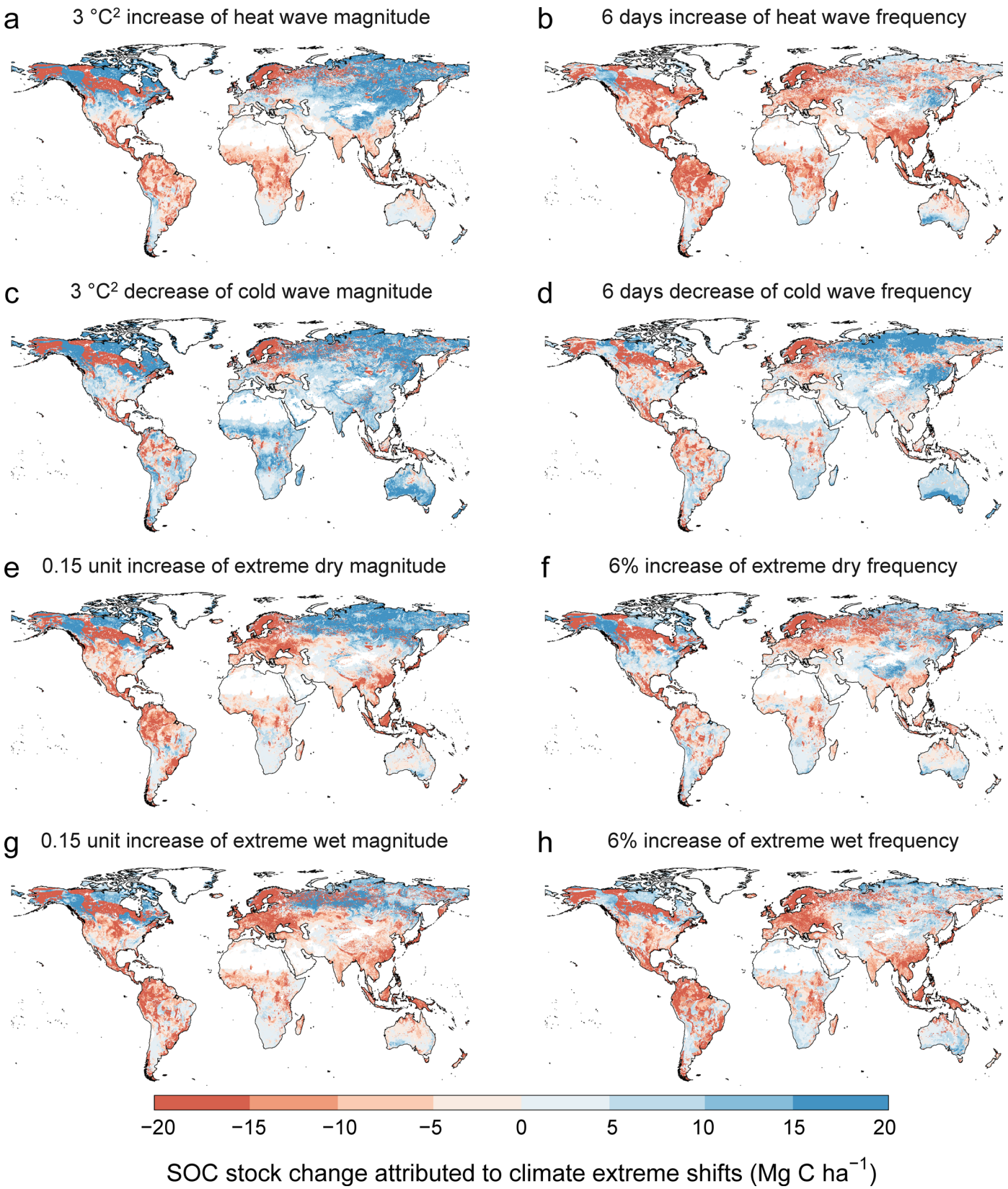

Extended Data Fig. 7 | The global spatial pattern of absolute changes in soil organic carbon stock under a warmer and more extreme climate. Global spatial pattern of absolute changes in soil organic carbon stock attributed to climate extreme shifts under a warmer and more extreme climate. **a-h**, eight climate extremes including heat wave magnitude (**a**) and frequency (**b**), cold wave magnitude (**c**) and frequency (**d**), extreme dry magnitude (**e**) and frequency (**f**), extreme wet magnitude (**g**) and frequency (**h**).

https://doi.org/10.1038/s41558-023-01874-3

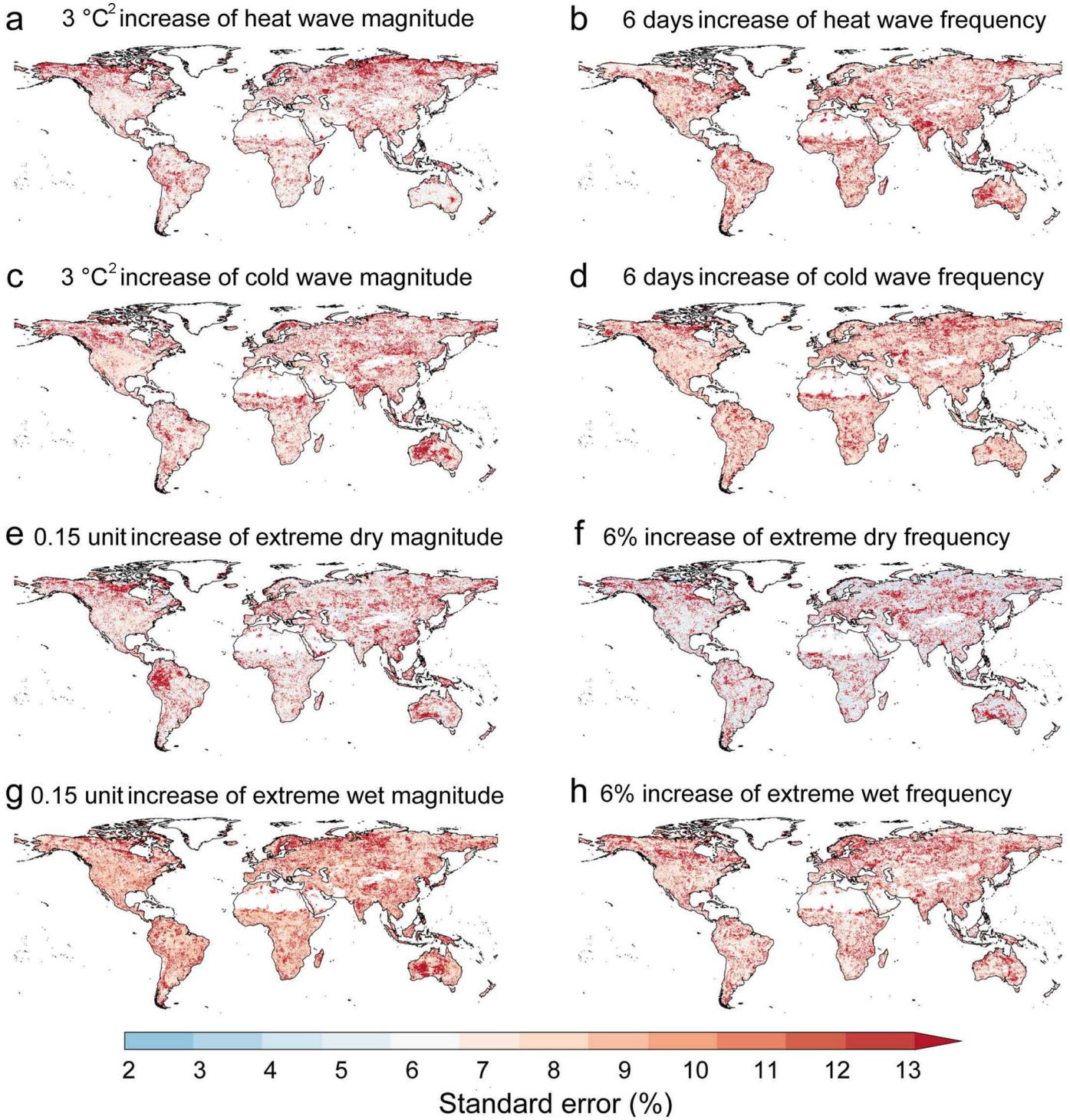

Extended Data Fig. 8 | The uncertainty of soil organic carbon relative changes under a warmer and more extreme climate. Uncertainty of soil organic carbon changes attributed to climate extreme shifts (ΔSOC_E) under a warmer and more extreme climate. ΔSOC_E is defined as the difference between percentage responses of SOC to W + E and that to W, which can also be explained as the additional changes in SOC induced by climate extremes. **a**-**h**, eight climate extremes including heat wave magnitude (**a**) and frequency (**b**), cold wave magnitude (**c**) and frequecy (**d**), extreme dry magnitude (**e**) and frequency (**f**), extreme wet magnitude (**g**) and frequency (**h**).

https://doi.org/10.1038/s41558-023-01874-3

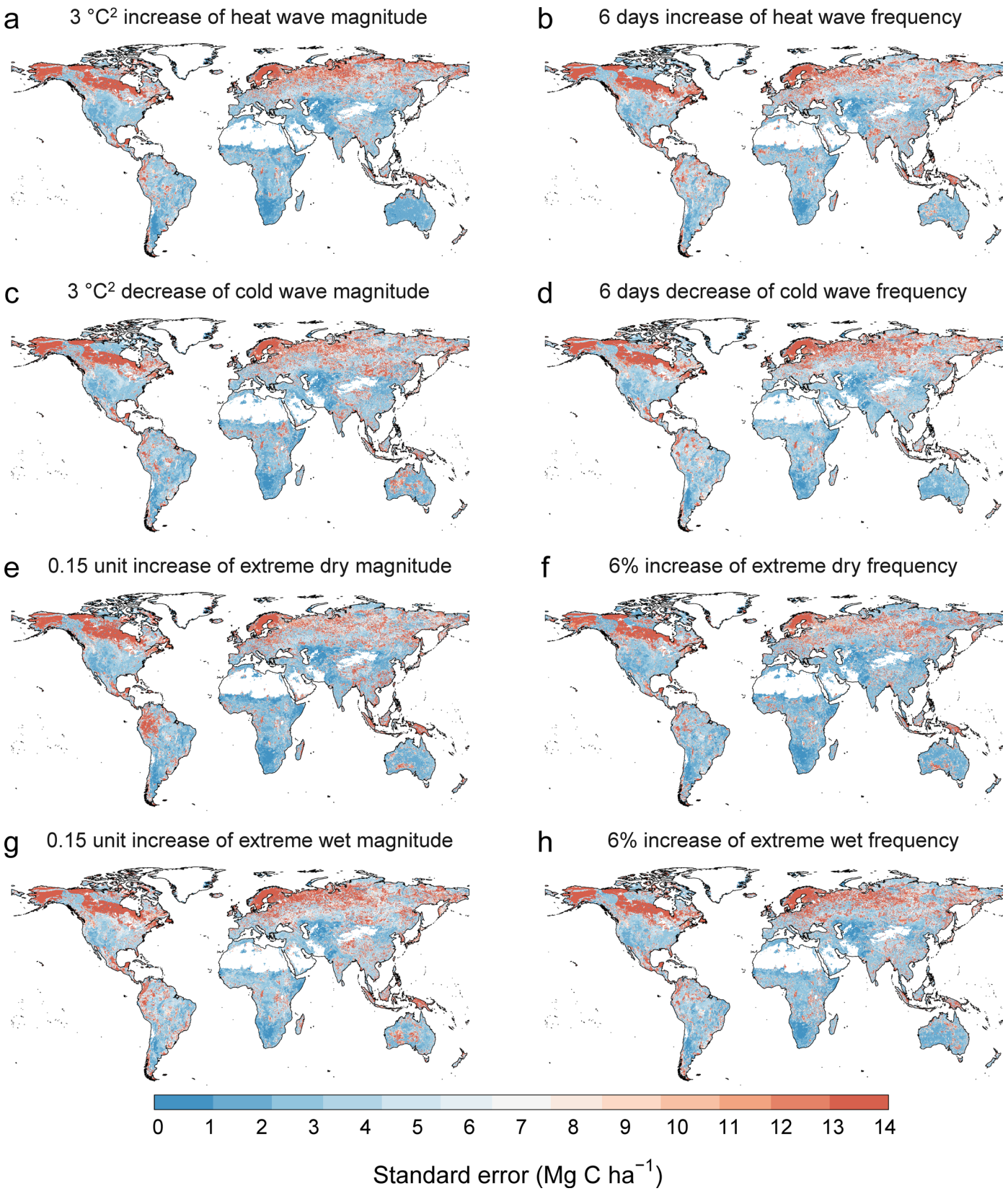

Extended Data Fig. 9 | The uncertainty of soil organic carbon absolute changes attributed to climate extreme shifts (ΔSOC_E, Mg C ha^{-1}) under a warmer and more extreme climate. The standard error was estimated based on 500 estimates of the random forest model. **a-h**, eight climate extremes including heat wave magnitude (**a**) and frequency (**b**), cold wave magnitude (**c**) and frequecy (**d**), extreme dry magnitude (**e**) and frequency (**f**), extreme wet magnitude (**g**) and frequency (**h**).

https://doi.org/10.1038/s41558-023-01874-3

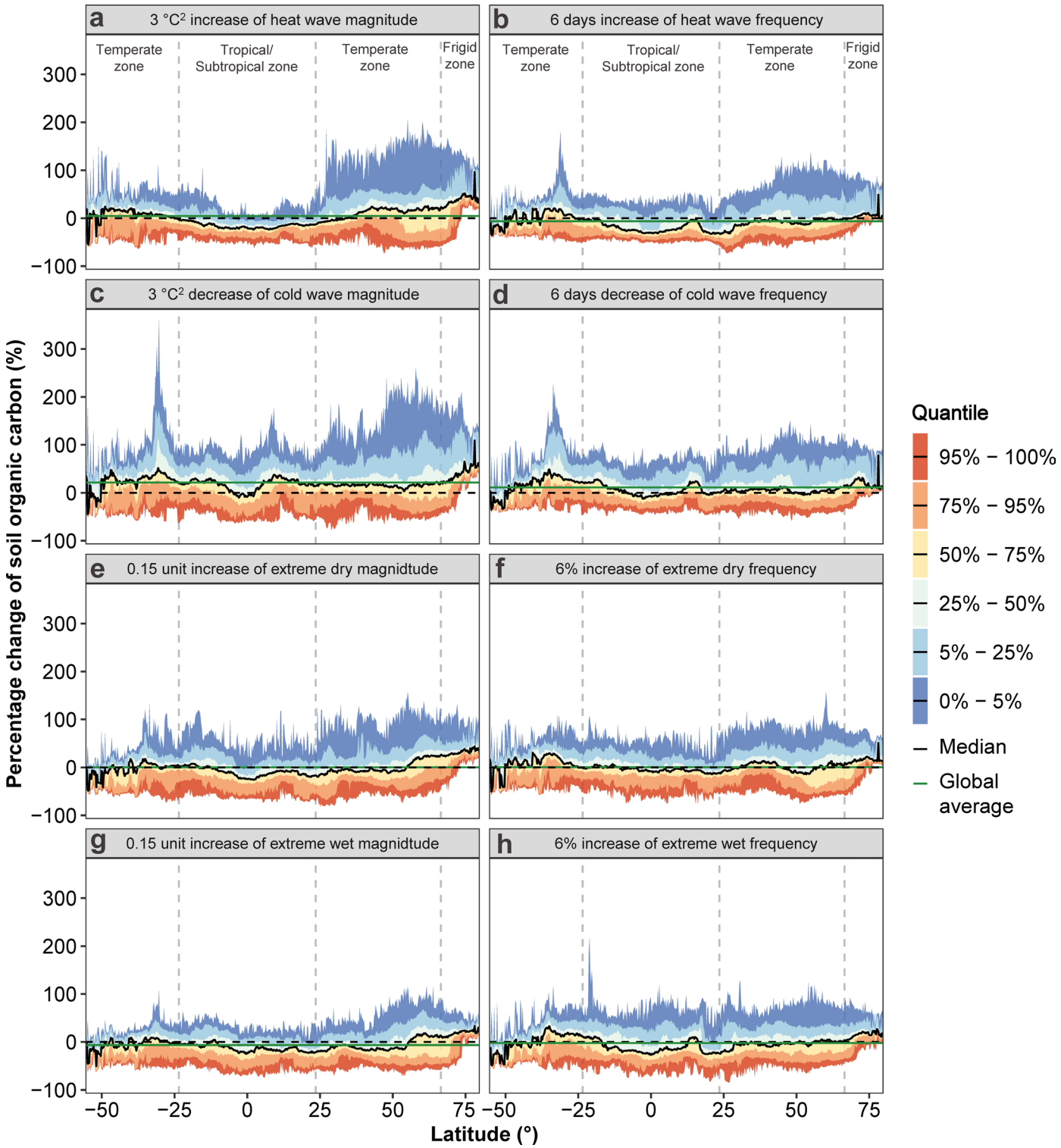

Extended Data Fig. 10 | The latitudinal pattern of changes in soil organic under 1.5 °C warming plus the specified climate change shifts. Latitudinal pattern of changes in soil organic carbon attributed to climate extremes (that is, ΔSOC_E) under 1.5 °C warming plus the specified climate change shifts. ΔSOC_E is defined as the difference between percentage responses of SOC to W + E and that to W, which can also be explained as the additional changes in SOC induced by climate extremes. **a-h**, eight climate extremes including heat wave magnitude (**a**) and frequency (**b**), cold wave magnitude (**c**) and frequecy (**d**), extreme dry magnitude (**e**) and frequency (**f**), extreme wet magnitude (**g**) and frequency (**h**). Black and green lines indicate the median and global average. Dashed lines show zero change, which is blocked by green lines in **e** and **f**.